# Oscillatory long-wave Marangoni convection in a layer of a binary liquid: Hexagonal patterns

S. Shklyaev,[1,2] A. A. Nepomnyashchy,[3,4] and A. Oron[5]

[1]*Department of Chemical Engineering, California Institute of Technology, Pasadena, California 91125, USA*

[2]*Institute of the Continuous Media Mechanics, Ural Branch of the Russian Academy of Sciences, Perm 614013, Russia*

[3]*Department of Mathematics, Technion-Israel Institute of Technology, Haifa 32000, Israel*

[4]*Minerva Center for Nonlinear Physics of Complex Systems, Technion-Israel Institute of Technology, Haifa 32000, Israel*

[5]*Department of Mechanical Engineering, Technion-Israel Institute of Technology, Haifa 32000, Israel*

(Received 19 June 2011; published 28 November 2011)

We consider a long-wave oscillatory Marangoni convection in a layer of a binary liquid in the presence of the Soret effect. A weakly nonlinear analysis is carried out on a hexagonal lattice. It is shown that the derived set of cubic amplitude equations is degenerate. A three-parameter family of asynchronous hexagons (AH), representing a superposition of three standing waves with the amplitudes depending on their phase shifts, is found to be stable in the framework of this set of equations. To determine a dominant stable pattern within this family of patterns, we proceed to the inclusion of the fifth-order terms. It is shown that depending on the Soret number, either wavy rolls 2 (WR2), which represents a pattern descendant of wavy rolls (WR) family, are selected or no stable limit cycles exist. A heteroclinic cycle emerges in the latter case: the system is alternately attracted to and repelled from each of three unstable solutions.

DOI: 10.1103/PhysRevE.84.056327 PACS number(s): 47.20.Dr, 47.54.−r, 47.20.Ky

## I. INTRODUCTION

Pattern formation and pattern selection remain a focus in the field of fluid dynamics and, particularly, in convection [1–3]. This problem is especially rich and thus complicated for an oscillatory mode. Theoretical treatment of pattern selection is possible only near the stability threshold, where the amplitude of convective motion is small. For a two-dimensional problem, this weakly nonlinear analysis results in the well-known complex Ginzburg-Landau amplitude equation [4]. For a three-dimensional case, a set of partial differential amplitude equations, similar to that obtained by Pomeau [5], has to be solved. The first important step in such an investigation is to consider a pattern selection on a fixed lattice, when the partial differential equations are replaced with ordinary ones. The complete analyses of the Hopf bifurcation on the square and hexagonal lattices are presented in Refs. [6,7], respectively. (The summary of Ref. [7] can be also found in Ref. [8].) In the latter case it is shown that sometimes the cubic, in terms of the amplitude of the convective motion, truncation of the set of amplitude equations is not sufficient, and due to degeneracy of the problem, the fifth-order terms have to be included.

Convection in a binary mixture is a well-known example of the system, where an oscillatory mode can emerge under certain conditions. We consider both thermo- and soluto-capillary convection in a layer of a binary fluid, choosing the same boundary conditions as in Ref. [9], where *long-wave oscillatory* mode was found. In general, an analysis of the long-wave mode is simpler than that for short waves, however a study of the long-wave oscillatory mode leads to the set of nonlocal equations, which, in turn, yields the conventional amplitude equations [6,7] following the Fourier transformation. Furthermore, as we show below, a novel degeneracy is inherent to the long-wave oscillatory instability on a hexagonal lattice for a wide class of problems. This degeneracy can be removed only in the presence of fifth-order nonlinear terms.

To the best of our knowledge, investigation of the pattern selection on a square lattice for the long-wave oscillatory mode in binary liquid was carried out only in three papers: In Refs. [10,11] buoyancy convection was studied, whereas in Ref. [12] Marangoni convection was explored. In both cases it was found that all patterns bifurcate supercritically and alternating rolls (AR) are the only stable pattern. A similar analysis for the Hopf bifurcation on a hexagonal lattice was presented in Ref. [13].

The present paper provides a detailed and extended description on this subject. Specifically, we shift a focus from general aspects of nonlinear dynamics [13] to the above-mentioned convection problem, thus paying much attention to construction of stability domains. Moreover, we consider stability of hexagonal patterns with respect to external perturbations that do not belong to the lattice.

The paper is organized as follows. In Sec. II we pose the problem and briefly reproduce main results of Refs. [9,12], necessary for the further analysis. In Sec. III we derive and explore the set of the amplitude equations with cubic nonlinearity. We find the novel degeneracy, which leads to the emergence of a three-parameter family of stable solutions. (One-parameter family is predicted by Roberts *et al.* [7].) In order to select the stable pattern among the above-mentioned three-parameter family, we proceed to the next order in Sec. IV, accounting for the quintic nonlinear terms. In the framework of the amplitude equations with fifth-order nonlinearity, we find several limit cycles and study their stability. In particular, we show that depending on the problem parameters, either wavy rolls 2 (WR2) is the only stable pattern or there is no stable pattern and heteroclinic cycle emerges. Separate analysis for the patterns, close to one of these limit cycles, alternating rolls (AR) on a hexagonal lattice is carried out in Sec. V. Numerical and analytical studies of the amplitude equations, presented in Sec. VI, confirm emergence of a heteroclinic cycle. Moreover, we construct the global map for the heteroclinic cycle, which shows that the cycle is attracting. In Sec. VII we perform the

 

stability analysis of the patterns forming the heteroclinic cycle with respect to external perturbations, which do not belong to the hexagonal lattice. It is shown that one of these patterns, AR, is unstable. We conclude in Sec. VIII.

## II. PROBLEM FORMULATION

### A. Governing equations

Referring to [9,12], we only briefly formulate the problem. Consider a horizontal planar binary-mixture layer of thickness $d_*$ at rest on a solid plate. The solid substrate is assumed to be of a low thermal conductivity and is heated from below, so that a constant temperature gradient $-a_*$ is prescribed at the substrate. (A more general problem where the heat flux in the substrate is accounted for was considered in Ref. [14].) The temperature gradient induces a gradient of the solute concentration through the Soret effect. The upper free boundary of the liquid layer is nondeformable and its surface tension depends on both temperature and solute concentration

$$\sigma_* = \sigma_0 - \sigma_t T_* + \sigma_c C_*, \tag{1}$$

where $\sigma_0$ is a reference value of the surface tension and $T_*$ and $C_*$ are small deviations of the temperature and concentration, respectively, from their reference values.

We take the Soret effect into account, thus defining the mass flux as

$$\mathbf{j} = -D_* \nabla (C_* + \alpha_* T_*),$$

where $D_*$ is the mass diffusivity and $\alpha_*$ is the Soret coefficient. The heat flux at the free surface is governed by Newton's law of cooling

$$-k_{\rm th} \nabla_n T_* = q_* T_*,$$

where $q_*$ and $k_{\rm th}$ are the heat transfer coefficient and the thermal conductivity of the liquid, respectively, and $\nabla_n$ is the gradient operator in the direction of the unit normal vector.

We choose $d_*^2/\kappa_*$, $d_*$, $a_* d_*$, $a_* d_* \sigma_t/\sigma_c$, $\kappa_*/d_*$, and $\rho_* \nu_* \kappa_*/d_*^2$ for the scales for time, length, temperature, solute concentration, velocity, and pressure fields, respectively. Here $\kappa_*$, $\nu_*$, and $\rho_*$ are the thermal diffusivity, kinematic viscosity, and density of the binary liquid, respectively. It should be noted that the time scale is different from that used in Refs. [9,12]. This change allows us to shorten several expressions and the corresponding changes in the governing equations are straightforward.

The fields of temperature and concentration are expressed as

$$\begin{aligned} T &= -z + \frac{B+1}{B} + \Theta(x,y,z,t), \\ C &= \chi z + C_0 + \Sigma(x,y,z,t), \end{aligned} \tag{2}$$

respectively. Thus, respective deviations $\Theta$ and $\Sigma$ from the equilibrium states of temperature and concentration are introduced. Here $z$ is the vertical spatial coordinate and $C_0$ is a constant whose value is not important for the further analysis and which is determined by the mean value of the solute concentration. Equation (2) contains two dimensionless numbers, the Biot number $B = q_* d_*/k_{\rm th}$ and the Soret number $\chi = \alpha_* \sigma_c/\sigma_t$.

The dimensionless boundary value problem governing the convective motion is

$$\nabla \cdot v = 0, \tag{3a}$$

$$P^{-1}(\mathbf{v}_t + \mathbf{v} \cdot \nabla \mathbf{v}) = -\nabla p + \nabla^2 \mathbf{v}, \tag{3b}$$

$$\Theta_t + \mathbf{v} \cdot \nabla \Theta - w = \nabla^2 \Theta, \tag{3c}$$

$$\Sigma_t + \mathbf{v} \cdot \nabla \Sigma + \chi w = L \nabla^2 (\Sigma + \chi \Theta), \tag{3d}$$

$$\mathbf{v} = \Theta_z = \Sigma_z = 0 \quad \text{at} \quad z = 0, \tag{4a}$$

$$\begin{gathered} w = 0, \quad \Theta_z + B\,\Theta = 0, \quad \Sigma_z - \chi B\,\Theta = 0, \\ \mathbf{u}_z = -M \nabla_2 (\Theta - \Sigma) \quad \text{at} \quad z = 1 \end{gathered} \tag{4b}$$

{compare with Eq. (30) in Ref. [9] keeping in mind the difference in the time scales}. Here $w$ is the vertical velocity component and $\mathbf{u}$ and $\nabla_2$ are two-dimensional (2D) projections of the velocity $\mathbf{v}$ and the gradient operator $\nabla$ onto the $x$-$y$ plane, respectively. Subscripts denote the partial derivatives with respect to the corresponding variables.

In addition to $B$ and $\chi$, the boundary-value problem Eqs. (3) and (4) contains three dimensionless parameters

$$M = \frac{\sigma_t a_* d_*^2}{\rho_* \nu_* \kappa_*}, \quad P = \frac{\nu_*}{\kappa_*}, \quad L = \frac{D_*}{\kappa_*},$$

which are the Marangoni, Prandtl, and Lewis numbers, respectively.

The above set of equations and boundary conditions admits a base state corresponding to the linear distribution of both temperature and concentration in a quiescent liquid, when $\Theta = \Sigma = \mathbf{v} = 0$.

### B. Long-wave expansion

The paper aims at the analysis of *hexagonal long-wave* perturbations to the base state. For the sake of reader convenience, we provide within this subsection a short summary of Refs. [9,12]. Only the results needed for the further analysis are presented. (Recall that the time scale is changed in comparison with the papers addressed.)

In order to study the dynamics of long-wave perturbations, we introduce stretched coordinates and velocities, fast and slow time variables (the necessity to introduce two time scales will be discussed below) via

$$X = \epsilon x, \quad Y = \epsilon y, \quad Z = z, \quad \mathbf{u} = \epsilon \mathbf{U}, \quad w = \epsilon^2 W, \tag{5a}$$

$$T = \epsilon^2 t, \quad \tau = \epsilon^4 t, \tag{5b}$$

where $\epsilon \ll 1$, and expand the Marangoni and Biot numbers

$$M = 48(m_0 + \epsilon^2 m_1 + \cdots), \quad B = \epsilon^4 \beta. \tag{6}$$

The last condition for the Biot number implies that the gas-liquid interface is nearly insulating.

The leading-order expressions for both temperature and solute concentration are independent of $Z$:

$$\Theta = F(X,Y,T,\tau) + O(\epsilon^2), \quad \Sigma = G(X,Y,T,\tau) + O(\epsilon^2),$$

whereas all other perturbations, such as those of the pressure and the fluid velocity, can be expressed via $F$, $G$, and $h \equiv F - G$. Obviously the value of $-h$ represents the perturbation of the surface tension. For instance, the leading-order components of

the velocity field induced by the deviation of surface tension are

$$\mathbf{U} = -12m_0 Z(3Z-2)\nabla h, \quad W = 12m_0 Z^2(Z-1)\nabla^2 h. \tag{7}$$

Hereafter $\nabla = (\partial_X, \partial_Y)$ denotes a rescaled 2D projection of the gradient operator onto the $X$-$Y$ plane.

The "fast," that is, with respect to time $T$, dynamics of the amplitude functions $F$ and $G$ is governed by the linear problem

$$L_1(F,G) \equiv F_T - (1-m_0)\nabla^2 F - m_0\nabla^2 G = 0, \tag{8a}$$

$$L_2(F,G) \equiv G_T - \chi(L+m_0)\nabla^2 F - (L-\chi m_0)\nabla^2 G = 0. \tag{8b}$$

According to Eqs. (8), the critical value of the Marangoni number for the oscillatory convection is given by

$$m_0 = \frac{1+L}{1+\chi}, \tag{9}$$

as obtained in Ref. [9]. At this value of the Marangoni number, the perturbed fields oscillate in $T$ with the frequency $\tilde{\Omega}$ proportional to the squared wave number $k$, whereas the growth (decay) of the perturbations occurs in the slow time $\tau$. Therefore, the general solution to Eqs. (8) can be written as

$$h = \sum_{\mathbf{k}} A_{\mathbf{k}}(\tau)\exp(i\mathbf{k}\cdot\mathbf{R} - i\tilde{\Omega}T) + \text{c.c.}, \tag{10}$$

$$F = \frac{m_0}{1-i\Omega}\sum_{\mathbf{k}} A_{\mathbf{k}}(\tau)\exp(i\mathbf{k}\cdot\mathbf{R} - i\tilde{\Omega}T) + \text{c.c.}, \tag{11}$$

$$G = F - h,$$

$$\tilde{\Omega} = \Omega k^2, \quad \Omega = \sqrt{-\frac{\chi(1+L+L^2)+L^2}{1+\chi}}. \tag{12}$$

Here $\mathbf{R} = (X,Y)$ is a two-dimensional radius vector and c.c. denotes the complex conjugate.

It is clear that $\Omega$ is real for $\chi_c > \chi > -1$, where $\chi_c = -L^2(1+L+L^2)^{-1}$. Under this condition, the long-wave oscillatory mode is critical within the long-wave approximation [9]. Competition between long-wave and short-wave perturbations was studied in Ref. [15]; it was shown that for $\chi > -0.1$, the long-wave oscillatory mode is critical. We consider below the long-wave oscillatory mode within this interval of the Soret number, $\chi_c > \chi > -0.1$.

Nonlinear dynamics of the amplitudes $A_{\mathbf{k}}$ in the slow time $\tau$ is governed by the following problem:

$$L_1(Q,R) = -F_\tau - \beta F - m_1\nabla^2 h - \frac{m_0}{60}\nabla^4\left[3\Phi - 2m_0\left(1+\chi+\frac{\chi}{L}\right)h\right] - \frac{m_0^2}{10}\nabla^2\left[\frac{1}{P}(\nabla h)^2 + 6\Gamma\right]$$
$$- \frac{m_0^2}{10}\left(1+\frac{2}{P}\right)\nabla\cdot(\nabla^2 h\nabla h) + \frac{48m_0^2}{35}\nabla\cdot[(\nabla h\cdot\nabla F)\nabla h] - \frac{312m_0^2}{35P}J(F,\psi), \tag{13a}$$

$$L_2(Q,R) = -G_\tau + \chi m_1\nabla^2 h + \frac{\chi m_0}{60}\nabla^4\left[3\Phi - 2m_0\left(1+\chi+\frac{\chi}{L}\right)h\right] + \frac{\chi m_0^2}{10}\nabla^2\left[\frac{1}{P}(\nabla h)^2 + 6\Gamma\right]$$
$$+ \frac{\chi m_0^2}{10}\left(1+L^{-1}+\frac{2}{P}\right)\nabla\cdot(\nabla^2 h\nabla h) - \frac{48m_0^2}{35}\nabla\cdot\{[\nabla h\cdot\nabla(\chi F - L^{-1}G)]\nabla h\} - \frac{312m_0^2}{35P}J(G,\psi), \tag{13b}$$

where $Q(X,Y,T,\tau)$ and $R(X,Y,T,\tau)$ can be thought as $O(\epsilon^2)$ corrections to $F$ and $G$, respectively,

$$\Gamma \equiv \nabla h\cdot\nabla[(1+\chi)F - L^{-1}G], \tag{14a}$$

$$\Phi \equiv \left[2 + \frac{m_0}{P}(1+\chi)\right]h - \frac{1-\chi L}{P}F + \frac{L}{P}G, \tag{14b}$$

$J(f,g) = f_X g_Y - f_Y g_X$ is a Jacobian of the mapping from $(X,Y)$ to $(f,g)$. The field $\psi$ is determined from

$$\nabla^2\psi = h_Y\nabla^2 h_X - h_X\nabla^2 h_Y, \tag{15}$$

and clearly represents a multiple of the toroidal potential of the velocity field.

In our calculations we set $\beta = 1$, which is equivalent to choosing $\epsilon = B^{1/4}$ in Eqs. (5) and (6), although in analytical expressions $\beta$ is kept.

The set of Eqs. (13a) and (13b) is a nonhomogeneous linear problem and the corresponding homogeneous problem [Eqs. (8)] has a nontrivial solution. Thus, one must determine the solvability conditions for Eqs. (13), which serve as evolution equations for the amplitudes $A_{\mathbf{k}}(\tau)$. Therefore, we deal with the *nonlocal* equations. At first glance, adding Eqs. (13a) and (13b) multiplied by $\epsilon^2$ to Eqs. (8a) and (8b), respectively, and replacing $F \to F + \epsilon^2 Q$ and $G \to G + \epsilon^2 R$, one reduces these nonlocal equations to local ones. However, as shown in Ref. [11], this "naive" way leads to incorrect results.

It is also noteworthy that Eqs. (8), as well as Eqs. (13), admit obvious spatially uniform (and, hence, independent of $T$) solutions $\langle F\rangle$ and $\langle G\rangle$. As follows from Eqs. (13),

$$\langle F\rangle_\tau = -\beta\langle F\rangle, \quad \langle G\rangle_\tau = 0.$$

Thus the mean temperature field decays in the slow time due to the heat flux from the free surface, whereas the mean value of the concentration does not evolve in $\tau$ at all. Bearing in mind that these parts do not interact with other Fourier harmonics, we set hereafter $\langle F\rangle = \langle G\rangle = 0$.

The linear stability problem in the framework of this approach results in a simple evolutionary equation:

$$\partial_\tau A_{\mathbf{k}} = \gamma A_{\mathbf{k}} \tag{16}$$

with the growth rate $\gamma$ given by

$$\gamma = \frac{m_1 k^2}{2}\left(1+\chi+i\frac{\chi+L+\chi L}{\Omega}\right) + \frac{m_0 k^4}{120P^2L}\left(f+i\frac{f_i}{\Omega}\right) - \frac{\beta}{2}\left(1+i\frac{L-\chi m_0}{\Omega}\right), \tag{17}$$

where

$$f = \chi[2P^2(1-L+L^2)-3PL(1+L)] + PL(-4P+2PL-3L), \tag{18a}$$

$$f_i = 2PL(\chi+L+\chi L)[3L-m_0(\chi+L+\chi L)] - 3L^2(1+\chi)\Omega^2. \tag{18b}$$

It is obvious that at $m_1 = m_1^{(0)}$,

$$m_1^{(0)} = \frac{1}{1+\chi}\left[\frac{\beta}{k^2} - \frac{m_0 f(\chi) k^2}{60P^2L}\right], \tag{19}$$

$\gamma_r$ vanishes. (Hereafter, the subscripts $r$ and $i$ denote the real and the imaginary parts of the corresponding complex variable, respectively.)

The function $m_1^{(0)}(k)$ has the only minimum $m_c$ at $k = k_c$, if $P\left(1+L^{-1}\right) > 3/2$, which is obviously true for most of liquid binary mixtures. (Recall, that the Lewis number $L$ is rather small.)

## III. AMPLITUDE EQUATIONS WITH CUBIC NONLINEARITY

### A. Weakly nonlinear expansion

Formally, Eqs. (13) are valid for any supercriticality $m_1 - m_c$ and, hence, for finite values of $h$. Such analysis would lead to extensive numerical computations. In contrast, bifurcation analysis on a *hexagonal* lattice can be studied at small supercriticality. To this end, we consider $m_1$ to be close to $m_c$ and set $k = k_c$; the subscript for the wave number is omitted. Below we only present the results for the field $h$, keeping in mind that both $F$ and $G$ can be expressed via Eq. (11).

For the sake of simplicity, we neglect the effects of a slow spatial modulation of the amplitudes and those of a mean flow induced by this modulation, dealing here with the perturbations of a fixed wave number only.

We consider hexagonal patterns beginning with the form of the field $h$ given by

$$h = \delta\big[A_1 e^{i\mathbf{K}^{(1)}\cdot\mathbf{R}} + A_2 e^{-i\mathbf{K}^{(1)}\cdot\mathbf{R}} + B_1 e^{i\mathbf{K}^{(2)}\cdot\mathbf{R}} + B_2 e^{-i\mathbf{K}^{(2)}\cdot\mathbf{R}} + C_1 e^{i\mathbf{K}^{(3)}\cdot\mathbf{R}} + C_2 e^{-i\mathbf{K}^{(3)}\cdot\mathbf{R}}\big]e^{-i\tilde{\Omega}T} + \text{c.c.} + O(\delta^3), \tag{20}$$

where

$$\mathbf{K}^{(1)} = (k,0), \quad \mathbf{K}^{(2,3)} = k\left(-\frac{1}{2}, \pm\frac{\sqrt{3}}{2}\right) \tag{21}$$

are the basis vectors of the hexagonal lattice.

Here $A_j$, $B_j$, $C_j$ are complex amplitude functions (from now on the subscript $j$ takes either of two values, 1 and 2), $\delta^2 \equiv m_1 - m_c \ll 1$ is a measure of supercriticality, and the wave number $k$ corresponds to the critical perturbations.

In order to perform the weakly nonlinear analysis on the hexagonal lattice, we introduce a multiscale expansion of the time derivative

$$\partial_\tau = \partial_{\tau_0} + \delta^2\partial_{\tau_1} + \delta^4\partial_{\tau_2} + \cdots$$

and expand the amplitudes into the series with respect to $\delta$:

$$(A_j, B_j, C_j) = \left(A_j^{(0)}, B_j^{(0)}, C_j^{(0)}\right) + \delta^2\left(A_j^{(1)}, B_j^{(1)}, C_j^{(1)}\right) + \cdots. \tag{22}$$

It should be emphasized that the above order of the limits $\epsilon \to 0$ (the long-wave expansion at small Biot number) and then $\delta \to 0$ (small-amplitude analysis) ensures the asymptotically exact results; it is known from Ref. [11] that these two limits do not commute for the long-wave oscillatory instability.

Below we treat the equations, which include *linear*, *cubic*, and *quintic* nonlinear terms as the problems at *zero*, *first*, and *second* orders in $\delta^2$, respectively.

The problem at *zero* order reads

$$\partial_{\tau_0} A_j^{(0)} = \gamma_0 A_j^{(0)}, \tag{23}$$

with similar two pairs of equations for $B_j^{(0)}$ and $C_j^{(0)}$. Here we represent the growth rate $\gamma$ [see Eq. (17)] in the form $\gamma = \gamma_0 + \delta^2\gamma_1$, where $\gamma_0 \equiv \gamma(m_1 = m_c)$ and $\gamma_1 \equiv \partial\gamma/\partial m_1$. (Hereafter we omit the argument $k$ for $\gamma$, if it does not lead to confusion.) It is obvious that $\gamma_0$ is imaginary, therefore the complex amplitudes $A_j^{(0)}$, $B_j^{(0)}$, and $C_j^{(0)}$ oscillate in $\tau_0$. The frequency of these oscillations, $\gamma_{0i}$, serves as a small correction to $\tilde{\Omega}$.

In the beginning of the nonlinear analysis, we recall that only "resonant" nonlinear terms, which satisfy the conditions

$$\mathbf{k} = s_1\mathbf{k}_1 + s_2\mathbf{k}_2 + s_3\mathbf{k}_3, \tag{24a}$$

$$k^2 = s_1 k_1^2 + s_2 k_2^2 + s_3 k_3^2, \tag{24b}$$

contribute to the nonlinear interaction. In such interaction three waves with their wave vectors $\mathbf{k}_1$, $\mathbf{k}_2$, $\mathbf{k}_3$ produce the wave with the wave vector $\mathbf{k}$ [10]. Here $s_j$ are either $\pm 1$ or zero.

The equations at *first* order yield a dynamical system for the complex amplitudes that consists of the pair of equations

$$\partial_{\tau_1} A_1 = A_1[\gamma_1 - K_0(|A_1|^2 + 2|A_2|^2) - K_1 N_{BC}] - K_2 A_2^*(B_1B_2 + C_1C_2), \tag{25a}$$

$$\partial_{\tau_1} A_2 = A_2[\gamma_1 - K_0(|A_2|^2 + 2|A_1|^2) - K_1 N_{BC}] - K_2 A_1^*(B_1B_2 + C_1C_2), \tag{25b}$$

$$N_{BC} \equiv |B_1|^2 + |B_2|^2 + |C_1|^2 + |C_2|^2 \tag{25c}$$

and of similar two pairs of equations for the rest of the amplitudes, which can be obtained based on Eqs. (25) by a cyclic permutation of $A$, $B$, and $C$. Hereafter the superscripts "(0)" for $A_j$, $B_j$, and $C_j$ are omitted, and the asterisk denotes the complex conjugate.

The coefficients of nonlinear interactions $K_n$ are

$$K_0 = \alpha_P + \beta_P, \quad K_1 = \frac{\alpha_P}{2} + \frac{5\beta_P}{4}, \quad K_2 = 2\alpha_P + \frac{\beta_P}{2}. \tag{26}$$

The expressions for the complex coefficients $\alpha_P$ and $\beta_P$, are given by Eqs. (37d) and (37e) in Ref. [12], respectively:

$$\alpha_P = \frac{24m_0^2k^4}{35L}\left[L + 1 + \frac{i}{\Omega}(L^2 + 1 - m_0)\right], \tag{27a}$$

$$\beta_P = -\frac{48m_0^2k^4}{35}\frac{i}{\Omega}. \tag{27b}$$

It is important to note that $\alpha_{Pr} > 0$ and $\beta_{Pr} = 0$.

The set of Eqs. (25) was analyzed by Roberts *et al.* [7] in order to study a Hopf bifurcation with a hexagonal symmetry. They found 11 limit cycles and studied their branching and stability. Besides, an additional pattern found by Swift [16] also exists under certain conditions and, thus, should be taken into account. A list of these limit cycles is given in Appendix A.

Before applying the results of Ref. [7] to the considered system, we must emphasize an additional symmetry property which is inherent to Eqs. (25) and (26). It is clear that the following relation:

$$3K_0 = 2K_1 + K_2 \tag{28}$$

is valid and this will be important for the further analysis since an additional degeneracy of Eqs. (25) ensues from it. It should be noted that Eq. (28) also holds for the buoyancy convection as well [10]. Moreover, as shown in Appendix B, the same relations are valid for a wide class of the problems, where long-wave oscillatory instability takes place. The only necessary conditions are the dispersion relation $\tilde{\Omega} \sim k^2$ and absence of the nonlinear terms involving $F$ and $G$ rather than their gradients (e.g., the analysis is invalid for the problem considered in Ref. [17], where the dispersion relation is quadratic in $k$, but one of the amplitude function is the surface deflection).

Equations (25) can be recast using Eq. (28) as

$$\partial_{\tau_1} A_1 = A_1[\gamma_1 - (K_0 - K_1)(|A_1|^2 - |A_2|^2)] - 2K_1 S A_1 - K_2 A_2^* \tilde{\Sigma}, \tag{29a}$$

$$\partial_{\tau_1} A_2 = A_2[\gamma_1 - (K_0 - K_1)(|A_2|^2 - |A_1|^2)] - 2K_1 S A_2 - K_2 A_1^* \tilde{\Sigma}, \tag{29b}$$

with two similar pairs of equations for $B_j$ and $C_j$. Here

$$2S = \sum_{j=1}^{2}(|A_j|^2 + |B_j|^2 + |C_j|^2), \tag{30a}$$

$$\tilde{\Sigma} = A_1A_2 + B_1B_2 + C_1C_2. \tag{30b}$$

In what follows we represent the complex amplitudes in the form

$$A_j = a_j e^{i\phi_{Aj}}, \quad B_j = b_j e^{i\phi_{Bj}}, \quad C_j = c_j e^{i\phi_{Cj}} \tag{31}$$

and by an appropriate choice of the origin and reference time, one has three conditions coupling the phases. Therefore, only three phase differences, for instance,

$$\Phi = \phi_{A1} + \phi_{A2} - \phi_{B1} - \phi_{B2}, \tag{32a}$$

$$\Psi = \phi_{A1} + \phi_{A2} - \phi_{C1} - \phi_{C2}, \tag{32b}$$

$$\Delta = \phi_{A1} - \phi_{A2} + \phi_{B1} - \phi_{B2} + \phi_{C1} - \phi_{C2} \tag{32c}$$

are essential. A set of the amplitude equations for nine real variables is presented in Appendix C, see Eqs. (C3) there.

It is noteworthy that the transformation excludes oscillation in $\tau_1$, thus the solutions are fixed points in the framework of Eqs. (C3). However, bearing in mind oscillation in $\tau_0$, we refer to these solutions as limit cycles.

It is also noted in Ref. [7] that the cubic equations are degenerate with respect to $\Delta$. Indeed, the set of Eqs. (25) is obviously invariant under transformation

$$A_2 \to e^{i\tilde{\psi}/3}A_2, \quad B_2 \to e^{i\tilde{\psi}/3}B_2, \quad C_2 \to e^{i\tilde{\psi}/3}C_2 \tag{33}$$

for any real $\tilde{\psi}$ and fixed $A_1$, $B_1$, $C_1$, when $\Delta$ is replaced with $\Delta - \tilde{\psi}$. This degeneracy can be removed only at the *second* order, when a quintic nonlinearity is introduced into the amplitude equations.

### B. Rolls, rhombic, and asymmetric patterns

It should be noted that $\Delta$ is unimportant for first eight limit cycles from the list in Appendix A, that is, for rolls, rhombic (rectangular) patterns, and for all the asymmetric patterns with either $a_1 \neq a_2$ or $b_1 \neq b_2$ or $c_1 \neq c_2$. For all these patterns at least two of the amplitudes vanish. Therefore there is no need in three phase differences $\Phi$, $\Psi$, and $\Delta$. The latter can be excluded by an appropriate choice of the point of origin, as well as at least one of $\Phi$ and $\Psi$.

Among these patterns there is no need in analyzing any rolls and rhombic patterns, as they have been already studied for an arbitrary angle $\theta$ between the wave vectors of interacting waves [12]. Therefore, we do not consider the following five patterns studied by Roberts *et al.* [7]: standing rolls (SR), traveling rolls (TR), standing rectangles (SRa with $\theta = \pi/3$), and traveling rectangles 1 and 2 (TRa1 with $\theta = 2\pi/3$ and TRa2 with $\theta = \pi/3$, respectively), which are supercritical and unstable even on the rhombic lattice. Moreover, standing cross rolls (SCR with $c_1 = c_2 = 0$, $a_1 = a_2 \neq b_1 = b_2$) do not exist on any rhombic lattice.

The remaining rhombic pattern found in Ref. [7] is alternating rolls (rectangular), AR-R, with $\theta = \pi/3$. (Below we abbreviate this pattern as AR.) This pattern is stable on a rhombic lattice and is neutrally stable on a hexagonal lattice, see Table 3.2 in Ref. [7] or Table 6 in Ref. [8], keeping in mind Eq. (26). This fact was also demonstrated in Sec. V C of Ref. [12].

To study other limit cycles in the framework of Eqs. (25), we begin from the *asymmetric* patterns with $a_1 \neq a_2$, $b_1 \neq b_2$, $c_1 \neq c_2$. It is clear from Appendix A that only oscillating triangles (OT)

$$a_1 = b_1 = c_1 = \sqrt{\frac{\gamma_{1r}}{2\alpha_{Pr}}}, \quad a_2 = b_2 = c_2 = 0 \tag{34}$$

have to be considered in addition to the above-mentioned seven rhombic patterns.

The phases $\phi_{A1}$, $\phi_{B1}$, and $\phi_{C1}$ of these three waves are not needed in the analysis as they are linear functions of $\tau_1$, whereas their differences can be eliminated by an appropriate choice of the origin. As $K_{0r} + 2K_{1r} = 2\alpha_{Pr} > 0$, this solution

bifurcates supercritically, while the condition $K_{2r} - K_{0r} = \alpha_{Pr} > 0$ enforces its instability in the entire parameter domain, see Table 3.2 in Ref. [7].

### C. Standing patterns: Limit cycles

We now proceed to the *standing* patterns with $a_1 = a_2 \equiv a$, $b_1 = b_2 \equiv b$, $c_1 = c_2 \equiv c$ that represent a superposition of three standing waves with different amplitudes and phases. Roberts *et al.* [7] found two one-parameter families of such patterns, namely

$$a = b = c = \sqrt{\frac{\gamma_{1r}}{9\alpha_{Pr}}}, \tag{35a}$$

$$\Phi = \Psi = 0, \tag{35b}$$

and

$$a = b = c = \sqrt{\frac{\gamma_{1r}}{3\alpha_{Pr}}}, \tag{36a}$$

$$\Phi = -\Psi = 2\pi/3. \tag{36b}$$

For these two families, variation in $\Delta$ results in a change of the patterns, that is, $\Delta$ serves as a parameter. The limiting cases of Eqs. (35) are the so-called standing hexagons (StH), $\Delta = 0$ and standing regular triangles (SRT) $\Delta = \pi$, while wavy rolls 2 (WR2) and twisted rectangles (TwR) are the representatives of the solutions given by Eqs. (36) corresponding to $\Delta = 0$ and $\Delta = \pi$, respectively.

Based on the results obtained by Roberts *et al.* [7] (see Table 3.2 there), one can readily see that some eigenvalues are positive in the first case [Eqs. (35)], whereas all eigenvalues are nonpositive in the second one [Eqs. (36)]. Moreover, for both cases three eigenvalues are zero. Vanishing one of them follows from the invariance under transformation (33) and this is known from Ref. [7]. The corresponding degeneracy is removed only at *second* order. Zero values of the other two eigenvalues indicate that some additional degeneracy takes place for the standing patterns. This novel degeneracy, intrinsic to the long-wave oscillatory mode, is a focal point of this paper.

To demonstrate this degeneracy, which is inherent to the *standing* patterns, it is more convenient to rewrite the set of Eqs. (C3) in terms of $S$ and $\hat{\Sigma}$ [see Eqs. (30)] as

$$\partial_{\tau_1} S = 2(\gamma_{1r} S - 2K_{1r} S^2 - K_{2r}|\hat{\Sigma}|^2), \tag{37a}$$

$$\partial_{\tau_1} \hat{\Sigma} = 2[\gamma_{1r} - (2K_{1r} + K_2)S + i\mathrm{Im}(K_2\hat{\Sigma})]\hat{\Sigma}, \tag{37b}$$

$$\partial_{\tau_1} \Phi = 2\mathrm{Im}[K_2\hat{\Sigma}(e^{i\Phi} - 1)], \tag{37c}$$

$$\partial_{\tau_1} \Psi = 2\mathrm{Im}[K_2\hat{\Sigma}(e^{i\Psi} - 1)], \tag{37d}$$

$$\partial_{\tau_1} \Delta = 0, \tag{37e}$$

where

$$\hat{\Sigma} = a^2 + b^2 e^{-i\Phi} + c^2 e^{-i\Psi} = \tilde{\Sigma} e^{-i(\phi_{A1} + \phi_{A2})}. \tag{38}$$

Note that $\hat{\Sigma}$ is complex and thus the second equation is also complex.

This set of amplitude equations has two different types of limit cycles. The first one corresponds to synchronous hexagonal patterns (SH)

$$\Phi = \Psi = 0, \quad S = \hat{\Sigma} = \frac{\gamma_{1r}}{3\alpha_{Pr}}. \tag{39}$$

Note that in general the amplitude of each standing wave is not uniquely determined by Eq. (39), that is, we obtain a two-parameter family of SH for any fixed $\Delta$. The particular case of this family with equal values of $a$,$b$, and $c$ corresponds to the above-mentioned StH and SRT. Other examples of SH are given by SRa (for $c = 0$) and SR ($b = c = 0$).

The second type corresponds to asynchronous hexagonal patterns (AH)

$$\hat{\Sigma} = 0, \quad S = \frac{\gamma_{1r}}{\alpha_{Pr}}, \tag{40}$$

written in terms of the amplitudes of standing waves $a$, $b$, and $c$ as

$$\begin{aligned} a^2 &= \mu_S \sin(\Psi - \Phi), \quad b^2 = -\mu_S \sin\Psi, \\ c^2 &= \mu_S \sin\Phi, \\ \mu_S &= \frac{S}{\sin(\Psi - \Phi) + \sin\Phi - \sin\Psi}. \end{aligned} \tag{41}$$

All complex amplitudes for AH oscillate as $\exp(-i\omega_1\tau_1)$ with the frequency determined by

$$\omega_1 = 2K_{1i}S - \gamma_{1i}, \tag{42}$$

which represents a nonlinear correction to $\tilde{\Omega}$.

The only limitations on the phase differences $\Phi$, $\Psi$ are the positivity conditions for $a^2$, $b^2$, $c^2$. Thus, Eq. (41) also defines a two-parameter family of solutions for any fixed $\Delta$ and with either

$$0 \leqslant \Phi \leqslant \pi, \quad -\pi \leqslant \Psi \leqslant \Phi - \pi \tag{43}$$

or

$$0 \leqslant \Psi \leqslant \pi, \quad -\pi \leqslant \Phi \leqslant \Psi - \pi. \tag{44}$$

Equation (41) shows that for fixed $\gamma_1$ and $\alpha_P$ (or, in other words, for fixed $S$), there exists a one-to-one correspondence between the two-parameter family of AH (with a fixed $\Delta$) and a family of triangles of a fixed perimeter $S$. The sides of each triangle $a^2$, $b^2$, and $c^2$ subtend the angles $\Phi - \Psi - \pi$, $\pi + \Psi$, and $\pi - \Phi$, respectively [see Fig. 1(a)].

The important representatives of the particular case of AH corresponding to isosceles triangles are:

(i) Symmetric patterns, $a^2 = b^2 = c^2$ or $\Phi = -\Psi = \Phi_0 \equiv \pm 2\pi/3$, corresponding to an equilateral triangle [Fig. 1(b)]. For $\Delta = 0$ and $\Delta = \pi$ symmetric patterns give rise to TwR and WR2, respectively.

The temporal evolution of the field $h$ during one-sixth of the oscillation period in the fast time $T$ in this particular case is depicted in Figs. 2(a) and 2(b) for $\Delta = 0$ and $\Delta = \pi$, respectively. Following this time interval, the initial distributions of $h$ are repeated with a clockwise rotation by $\pi/3$. Figure 2(a) shows the transition between hexagonal patterns to the rhombic ones and then again transition back to hexagons, while in Fig. 2(b) rhombic patterns alternate with triangles.

(ii) AH with a vanishing amplitude of one of the standing waves; either AR-A with $a = 0$ and $\Phi - \Psi = \pi$, or AR-B with $b = 0$ and $\Psi = -\pi$, or AR-C with $c = 0$ and $\Phi = \pi$. Therefore, AH reduces to AR on a hexagonal lattice. This pattern is described by an isosceles triangle with almost right base angles [see Fig. 1(c)]. The temporal evolution of $h$ in

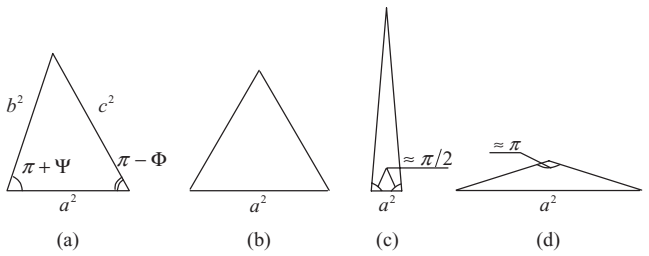


FIG. 1. Triangles of a fixed perimeter corresponding to the family of AH: (a) general case; (b) equilateral triangle, $\Phi = -\Psi = 2\pi/3$ or $a = b = c$ corresponding to symmetric patterns; (c) isosceles triangle with a zero angle subtending the base, which corresponds to AR, $\Phi - \Psi = \pi$ or $a = 0$; and (d) isosceles triangle with zero base angles, corresponding to the family of OHR, $\Phi = -\Psi = \pi$ or $a^2 = 2b^2 = 2c^2$.

this case is shown in Fig. 3 during a quarter of a period. The pattern evolves from the rolls oriented normally to $\mathbf{K}^{(2)}$ into a rectangular pattern and then into rolls oriented normally to $\mathbf{K}^{(3)}$.

(iii) Oscillating hexarolls (OHR) $\Phi = -\Psi = \pi$, corresponding to degenerate triangles with the angles 0, 0, $\pi$ [see Fig. 1(d)].

For these patterns the amplitude of one standing wave is maximal, that is, $a^2 = 2b^2 = 2c^2$. The field $h$ can be rewritten as follows:

$$h = 2\left[\sqrt{2}\cos kX\cos\tilde{\Omega}T - 2\sin\left(\frac{1}{2}kX + \frac{3}{4}\Delta\right)\sin\frac{\sqrt{3}}{2}kY\sin\tilde{\Omega}T\right]. \quad (45)$$

Evolution of $h$ in the fast time $T$ for two particular cases of OHR, $\Delta = 0$ (OHR1) and $\Delta = \pi$ (OHR2), is shown in Fig. 4.

### D. Linear stability of standing patterns

Linear stability analysis of the solutions given by Eqs. (39) and (40) shows that SH are unstable, while all AH are stable in the framework of a symmetrized set of Eqs. (37). The results of the stability analysis are presented in Table I. [In fact, for SH Eqs. (29) are applied rather than Eqs. (37): $S = \hat{\Sigma}$ at

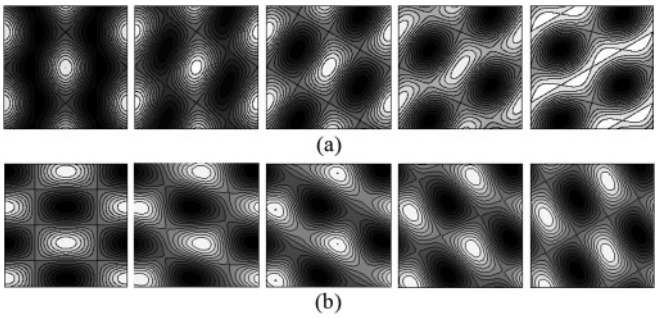


FIG. 2. Temporal evolution of $h$ for $\tilde{\Omega}T = 0, \pi/12, \pi/6, \pi/4, \pi/3$ (left to right) for AH with $a = b = c$. The horizontal and vertical axes are, respectively, $X$ and $Y$. (a) $\Delta = 0$ (TwR). (b) $\Delta = \pi$ (WR2).

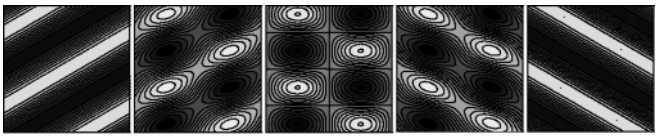

FIG. 3. Temporal evolution of $h$ for $\tilde{\Omega}T = 0, \pi/8, \pi/4, 3\pi/8, \pi/2$ (left to right) for AR-A. The horizontal and vertical axes are, respectively, $X$ and $Y$.

$\Phi = \Psi = 0$ and therefore Eqs. (37a) and (37b) coincide with each other; moreover, two zero eigenvalues corresponding to arbitrary choice of $a^2$, $b^2$, and $c^2$ at fixed $S$ are lost within Eqs. (37).] One can see that there exist two unstable eigenvalues for SH and there are no unstable eigenvalues for AH. It is shown in Appendix C that AH are stable even in the framework of a more general problem governed by Eqs. (25) [or Eqs. (C3)], that is, when at least one out of the symmetry conditions $a_1 = a_2$, $b_1 = b_2$, or $c_1 = c_2$ is violated.

Thus, a three-parameter family of limit cycles (AH) is stable in the framework of Eqs. (25). Only the phases $\phi_{A1,2}$, $\phi_{B1,2}$, and $\phi_{C1,2}$ linearly evolve in $\tau_1$ according to Eq. (42), whereas the amplitudes $a$, $b$, and $c$ and the phase differences $\Phi$, $\Psi$, and $\Delta$ are constant. Using Eq. (41) it is possible to express the values of the amplitudes of the standing waves via the phase differences $\Phi$ and $\Psi$.

We solved Eqs. (25) numerically and showed that for any set of initial conditions, the solution evolves to one of the limit cycles of a three-parameter family of AH with no other solutions found. It is possible to reproduce any solution given by Eq. (41) by variation of the initial conditions.

Hence, in order to select stable patterns within the above-mentioned family of limit cycles, it is necessary to perform a more general analysis of *standing* patterns based on the set of Eqs. (25) extended to include the quintic nonlinear terms.

## IV. INCLUSION OF THE FIFTH-ORDER TERMS

### A. Derivation of amplitude equations

To select the stable pattern among AH, we must take fifth-order nonlinear terms into account. It is shown in Sec. III C

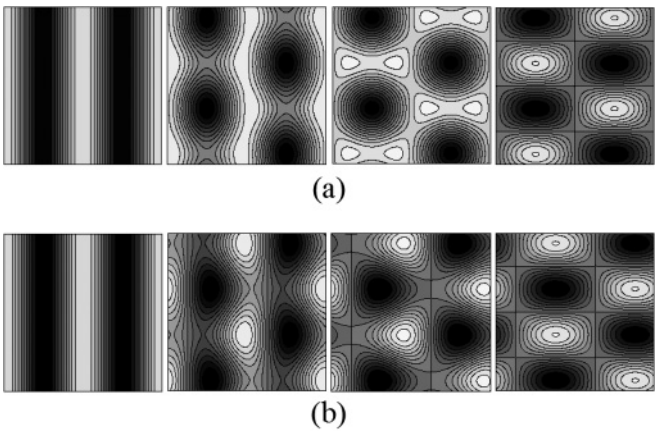


FIG. 4. Temporal evolution of $h$ for $\tilde{\Omega}T = 0, \pi/8, \pi/4, 3\pi/8, \pi/2$ (left to right) for AH with $a^2 = 2b^2 = 2c^2$. The horizontal and vertical axes are, respectively, $X$ and $Y$. (a) $\Delta = 0$ (OHR1). (b) $\Delta = \pi$ (OHR2).

TABLE I. Growth rates for limit cycles in the framework of Eqs. (37). The second column shows the eigenvalues $\lambda$ for the limit cycles. The third column shows the eigenfunction corresponding to the respective eigenvalue $\lambda$; for instance, for SH perturbation of $S$ (or $\hat{\Sigma}_r$) evolves according to $\exp(-2\gamma_{1r}\tau_1)$, whereas $\Phi$ grows as $\exp(4\gamma_{1r}\tau_1/3)$, as follows from the first and the fourth rows, respectively.

| Pattern | $\lambda$ | Eigenfunction |
|---|---|---|
| SH | $-2\gamma_{1r}$ | $S$ or $\hat{\Sigma}_r$ |
| | 0 | $\Delta$ |
| | 0 | $a^2$, $b^2$, $c^2$ |
| | $2K_{2r}S$ | $\Phi$ |
| | $2K_{2r}S$ | $\Psi$ |
| AH | $-2\gamma_{1r}$ | $S$ |
| | $-2K_2S$, $-2K_2^*S$ | $\hat{\Sigma}_r$, $\hat{\Sigma}_i$ |
| | 0 | $\Phi$ |
| | 0 | $\Psi$ |
| | 0 | $\Delta$ |

that according to Eqs. (37), the phase differences $\Phi$ and $\Psi$ do not evolve in time $\tau_1$. To determine the evolution of $\Phi$, $\Psi$, and $\Delta$, and therefore via Eq. (41), $a$, $b$, and $c$, in the slow time $\tau_2$, we proceed to the *second* order of expansion in $\delta^2$, accounting thus for the quintic nonlinear terms.

First, we describe the emergence of $O(\delta^3)$ nonlinear terms in $h$ in the amplitude equation at *first* order, that is, via cubic nonlinearities. The wave set with the wave vectors $\mathbf{k}_1 = \mathbf{k}_2 = \mathbf{K}^{(2)}$, $\mathbf{k}_3 = \mathbf{K}^{(1)}$, and $\mathbf{k} = \sqrt{3}k(0,1) = \mathbf{K}^{(2)} - \mathbf{K}^{(3)}$ clearly satisfies the resonant conditions [Eqs. (24)] with $s_1 = s_2 = s_3 = 1$. [Recall that the base vectors of the lattice are given by Eq. (21).] Thus, the generation of the wave proportional to $D_1 \exp[i(\sqrt{3}kY - 3\tilde{\Omega}T)]$ should be accounted for. Below for the sake of brevity, we refer to such interaction as $B_1 + B_1 + A_1 \to D_1$. (Of course $D_1$ can be also produced via the interaction $C_2 + C_2 + A_2 \to D_1$.) Therefore, we must complete the representation of $h$, given by Eq. (20), adding the following six terms:

$$\delta^3 D_1 \exp[i(\sqrt{3}kY - 3\tilde{\Omega}T)] + \text{r.t.}, \tag{46}$$

where "r.t." denotes five additional waves with the amplitudes $D_l$ ($l = 2, \ldots, 6$), produced by rotating the wave presented in Eq. (46) by the angles $(l-1)\pi/3$ (see Fig. 5).

It is easy to see that the dynamics of $D_1$ is governed by the equation

$$\partial_{\tau_0} D_1 = \Gamma_3 D_1 - K_3\left(A_1 B_1^2 + A_2 C_2^2\right),$$

where $\Gamma_3 \equiv \gamma_0(\sqrt{3}k)$, $K_3 = 3\alpha_P/2$. The steady solution is

$$D_1 = \frac{K_3\left(A_1 B_1^2 + A_2 C_2^2\right)}{\Gamma_3 - 3\gamma_0} \tag{47}$$

and similar expressions can be obtained for the other five amplitudes. (Recall that $\gamma_0$ is purely imaginary.)

The six additional terms also lead to the emergence of additional resonant terms, for instance, through the interaction $D_1 - B_1 - B_1 \to A_1$. The coefficient of the nonlinear interaction is $K_4 = -3\beta_P/4$. [The resonant conditions (24) are met for $\mathbf{k}_1 = k(0, \sqrt{3})$, $\mathbf{k}_2 = \mathbf{k}_3 = \mathbf{K}^{(2)}$ with $s_1 = 1$, $s_2 = s_3 = -1$.] Accounting for all interactions of such kind, results in the set of equations at second order:

$$\begin{aligned}\partial_{\tau_1} A_1^{(1)} &= \hat{L}_{A1} - \dot{A}_1 - \kappa(c^4 + b^4)A_1 \\ &\quad - \kappa[(C_1^* B_2)^2 + (B_1^* C_2)^2]A_2, \qquad (48a)\\ \partial_{\tau_1} A_2^{(1)} &= \hat{L}_{A2} - \dot{A}_2 - \kappa(c^4 + b^4)A_2 \\ &\quad - \kappa[(C_2^* B_1)^2 + (B_2^* C_1)^2]A_1, \qquad (48b)\end{aligned}$$

and with similar four equations for the other amplitudes. In Eqs. (48) we use the expansion for the complex amplitudes [Eqs. (22)], a dot denotes the derivative with respect to $\tau_2$ and

$$\begin{aligned}\hat{L}_{A1} &\equiv -2A_1\left[\sigma \mathrm{Re}\left(A_1^* A_1^{(1)} - A_2^* A_2^{(1)}\right)\right] \\ &\quad - 2K_1 S_1 A_1 - K_2 A_2^* \tilde{\Sigma}_1, \qquad (49a)\\ \hat{L}_{A2} &\equiv 2A_2\left[\sigma \mathrm{Re}\left(A_1^* A_1^{(1)} - A_2^* A_2^{(1)}\right)\right] \\ &\quad - 2K_1 S_1 A_2 - K_2 A_1^* \tilde{\Sigma}_1, \qquad (49b)\end{aligned}$$

$\kappa \equiv K_3 K_4/(\Gamma_3 - 3\gamma_0) = -9\alpha_P\beta_P/8(\Gamma_3 - 3\gamma_0)$, $\sigma \equiv K_0 - K_1$, and the expansions $S = S_0 + \delta^2 S_1$, $\tilde{\Sigma} = \delta^2\tilde{\Sigma}_1$ are used, that is,

$$S_1 = \mathrm{Re}\sum_{j=1}^{2}\left(A_j^* A_j^{(1)} + B_j^* B_j^{(1)} + C_j^* C_j^{(1)}\right), \tag{50a}$$

$$\tilde{\Sigma}_1 = A_1 A_2^{(1)} + A_2 A_1^{(1)} + B_1 B_2^{(1)} + B_2 B_1^{(1)} + C_1 C_2^{(1)} + C_2 C_1^{(1)}. \tag{50b}$$

Other nonlinear terms predicted in Ref. [7], such as

$$A_2 B_1^* B_2 C_1^* C_2 \tag{51}$$

and

$$A_1^2 A_2 (B_1^* B_2^* + C_1^* C_2^*) \tag{52}$$

do not influence the dynamics at second order. Indeed, Eqs. (13) contain only quadratic and cubic nonlinear terms, that is, the sole way to produce the quintic nonlinearity is the generation of a certain "virtual" wave. However, simple enumeration indicates that no triad of waves, which enter

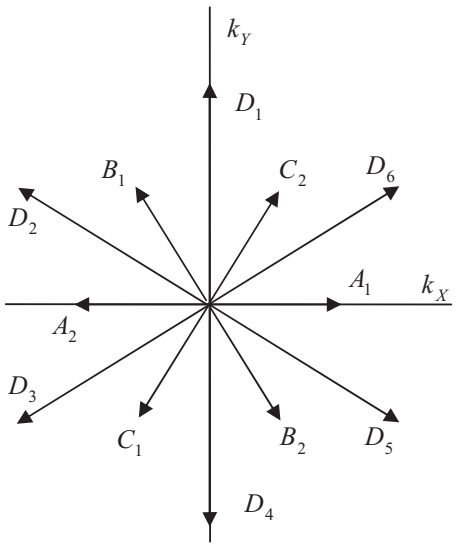


FIG. 5. Wave vectors of interacting perturbations on the hexagonal lattice.

into Eqs. (51) or (52), meets the resonant conditions [Eqs. (24)]. The only exception is the simplest generation of, say, $B_2$ within the resonant interaction $A_1 + A_2 - B_1 \to B_2$ and then the inclusion of this virtual wave in the interaction of type $A_1 + B_2 - B_2 \to A_1$. However, both these nonlinear interactions have been already taken into account in Eqs. (25) and (48). As for the quadratic interaction, they are obviously unimportant for the hexagonal lattice.

Assuming that $A_j^{(1)} = a_j \exp(i\phi_{Aj})$ with similar expressions for the other amplitudes, we eliminate the amplitudes deriving the following set of equations:

$$\dot{\Phi} = 2\frac{c^2}{S_0}\mathrm{Im}(Fe^{-i\Psi})(1 - 2\cos\Delta), \tag{53a}$$

$$\dot{\Psi} = -2\frac{b^2}{S_0}\mathrm{Im}(Fe^{-i\Phi})(1 - 2\cos\Delta), \tag{53b}$$

$$\dot{\Delta} = -2Q(a^4 + b^4 + c^4)\sin\Delta, \tag{53c}$$

where

$$F = \kappa[(b^4 - a^4)(1 - e^{i\Psi}) - (c^4 - a^4)(1 - e^{i\Phi})], \qquad Q = \frac{\mathrm{Re}(\sigma\kappa^*)}{\sigma_r}. \tag{54}$$

The amplitudes $a$, $b$, and $c$ depend on the slowest time $\tau_2$ only via the phases according to Eq. (41). In other words, relaxation of the amplitudes in $\tau_1$ is "fast" and Eq. (41) is valid during the evolution in $\tau_2$. It should be emphasized that Eqs. (53) are valid only if all the amplitudes $a$, $b$, and $c$ are of the same order of magnitude. The cases of ARs and close patterns with, say, $a \ll \min(b,c)$ are analyzed in Sec. V.

For the sake of brevity we set $S_0 = 1$, which can be achieved by rescaling the slow time $\tau_2$, or, even by a more natural rescaling of the parameter $\delta$: $\delta^2 S_0 \to \delta^2$. Therefore, hereafter it is assumed accordingly $a^2 + b^2 + c^2 = 1$.

### B. Limit cycles

It can be readily shown that there exist five stationary points of Eqs. (53) which are limit cycles in the framework of the full set of equations. They are:

(i) and (ii) Symmetric patterns, TwR and WR2, with $\Phi = -\Psi = \Phi_0 \equiv \pm 2\pi/3$, that is, $a = b = c$. Recall that $\Delta = 0$ for TwR and $\Delta = \pi$ for WR2. (The list of acronyms for patterns revealed by Roberts *et al.* [7] is given for the reader's convenience in Appendix A.)

(iii) Alternating rolls (ARs): $\Phi - \Psi = \pi$, that is, $a = 0$, $b = c \neq 0$ (AR-A). There also exist two similar patterns with either $b = 0$ (AR-B) or $c = 0$ (AR-C).

(iv) and (v) Oscillating hexarolls (OHR) with $\Phi = -\Psi \to \pi$, that is, $a^2 = 2b^2 = 2c^2$ and either $\Delta = 0$ (OHR1) or $\Delta = \pi$ (OHR2). Again, two similar pairs of patterns exist with either $b$ or $c$ being the dominant amplitude.

The corresponding evolution of $h(T)$ for these five solutions is presented in Figs. 2–4. The results of the linear stability analysis of these limit cycles are summarized in Table II, where the growth rates $\lambda$ and conditions of stability are presented.

Note that $Q$ determines the dynamics of $\Delta$ when $\Phi$ and $\Psi$ are fixed. For all patterns with $\Delta = 0$, the instability condition is $Q < 0$, whereas for $\Delta = \pi$ the instability condition is $Q > 0$. In particular, for the symmetric patterns TwR and WR2, these conditions coincide with those obtained by Roberts *et al.* [7], see the last row for TwR and WR2 in Table 3.2 there.

TABLE II. Growth rates for limit cycles in the framework of Eqs. (53). The third column indicates the stability (+) or instability (−) for $Q > 0$ (the upper sign) and for $Q < 0$ (the lower sign), see Fig. 7.

| Pattern | $\lambda$ | Stability | Manifold |
|---|---|---|---|
| (i) TwR | $-\frac{2}{9}\kappa$, $-\frac{2}{9}\kappa^*$ | − | $\Delta = 0$ |
| | $-\frac{2Q}{3}$ | +/− | $\Phi = -\Psi = \Phi_0$ |
| (ii) WR2 | $\frac{2}{3}\kappa$, $\frac{2}{3}\kappa^*$ | + | $\Delta = \pi$ |
| | $\frac{2Q}{3}$ | −/+ | $\Phi = -\Psi = \Phi_0$ |
| (iii) AR | $\frac{1}{2}\kappa_r$ | + | $\Delta = 0$ |
| | $-\frac{3}{2}\kappa_r$ | − | $\Delta = \pi$ |
| | $-Q$ | +/− | $a^2 = 0, \Delta = 0$ |
| | $Q$ | −/+ | $a^2 = 0, \Delta = \pi$ |
| (iv) OHR1 | $-\frac{3}{16}\kappa_r$ | − | $\Delta = 0, b = c$ |
| | 0 | − | $\Delta = 0, b \neq c$ |
| | $-\frac{3Q}{4}$ | +/− | $\Phi = -\Psi = \pi$ |
| (v) OHR2 | $\frac{9}{16}\kappa_r$ | + | $\Delta = \pi, b = c$ |
| | 0 | − | $\Delta = 0, b \neq c$ |
| | $\frac{3Q}{4}$ | −/+ | $\Phi = -\Psi = \pi$ |

It is worth noting that the representation of ARs in terms of $\Phi$ and $\Psi$ is inadequate, since ARs are not even fixed points of Eqs. (53). Indeed, for AR-A ($b^2 \approx c^2 \approx \frac{1}{2}$, $a^2 \to 0$) the approximate expression

$$F \approx \tfrac{1}{2}\kappa e^{i\Phi} \tag{55}$$

is valid. Thus, only the difference $\Phi - \Psi$ is fixed, whereas each of these phase variables grows linearly with $\tau_2$:

$$\Phi \approx -\tfrac{1}{2}(1 - 2\cos\Delta_0)\kappa_i\tau_2, \quad \Psi \approx -\pi + \Phi. \tag{56}$$

(Recall that the value of $\Delta$ is not important for ARs, although formally only either $\Delta = 0$ or $\Delta = \pi$ correspond to a fixed point.) Due to Eq. (55) and the obvious relation

$$\dot{\Phi} - \dot{\Psi} = -2a^2 F_i(1 - 2\cos\Delta),$$

which follows from Eqs. (53a) and (53b), one obtains for the perturbations:

$$\partial_{\tau_2} a^2 = -\tfrac{1}{2}\kappa_r(1 - 2\cos\Delta)a^2. \tag{57}$$

The growth rates for $a^2$ at $\Delta = 0, \pi$ are shown in the first two rows of Table II for ARs. The second pair of rows presents the result of linearization of Eq. (53c) around the two values of $\Delta$ at $a = 0$, $b^2 = c^2 = \frac{1}{2}$.

Recall that $\Delta$ is unimportant for ARs and the fact that $\Delta$ changes the stability of ARs (cf. $\Delta = 0$ and $\Delta = \pi$) should be explained. In fact, the pattern with $a \ll \min(b,c)$ is not an exact AR and Eqs. (53) should be rewritten when one among the standing waves becomes rather small. This routine described in Sec. V provides the internal solution which should be matched with the external one, that is, the solution of Eqs. (53). In terms of Eqs. (53), this routine transforms the trajectory close to the stable manifold for AR, $\Delta = 0$, to the initial condition

near the unstable manifold, $\Delta = \pi$, that is, provides details of attraction to AR and repelling from this fixed point.

It should be also emphasized that both OHR1 and OHR2 are neutrally stable with respect to perturbations with $b \neq c$ in the framework of linear stability theory. However, inclusion of nonlinear terms results in instability of both OHR1 and OHR2. Indeed, introducing

$$\Phi = \pi - \epsilon_1, \quad \Psi = -\pi + \epsilon_2, \quad \min(\epsilon_1,\epsilon_2) > 0, \quad (58)$$

equivalent to

$$a^2 = \frac{1}{2}, \quad b^2 = \frac{\epsilon_1}{2(\epsilon_1+\epsilon_2)}, \quad c^2 = \frac{\epsilon_2}{2(\epsilon_1+\epsilon_2)}, \quad (59)$$

one can readily obtain

$$\dot\epsilon_1 = R\frac{\epsilon_1(\epsilon_1-\epsilon_2)}{(\epsilon_1+\epsilon_2)^2}, \quad \dot\epsilon_2 = R\frac{\epsilon_2(\epsilon_1-\epsilon_2)}{(\epsilon_1+\epsilon_2)^2}, \quad (60)$$

where $R = \frac{1}{2}\kappa_i(1-2\cos\Delta)$. Substituting $X_1 \equiv \epsilon_1+\epsilon_2$ and $X_2 \equiv \epsilon_1-\epsilon_2$, we find

$$\dot X_1 = R\frac{X_2}{X_1}, \quad \dot X_2 = R\frac{X_2^2}{X_1^2}. \quad (61)$$

The solution of this set of equations reads

$$X_1 = C^2|\tau_2-\tau_{20}|, \quad X_2 = \frac{C^4}{R}(\tau_2-\tau_{20}), \quad (62)$$

where $C$ and $\tau_{20}$ are arbitrary constants. Thus, both OHR1 and OHR2 ($X_1 = X_2 = 0$) are unstable; the system approaches each of these limit cycles and leaves it in a finite time. This is why in the third column of Table II both OHR1 and OHR2 are marked as unstable. Therefore, we do not discuss these patterns any further.

### C. Domains of stability

It follows from Table II that the signs of $\kappa_r$ and $Q$ are important for stability of the patterns. When $\kappa_r Q > 0$, one of the *symmetric* patterns (WR2 or TwR) is stable, whereas the remaining four patterns are unstable. The system governed by Eqs. (53) approaches the sole stable solution. More precisely, for $\kappa_r < 0$ and $Q < 0$, WR2 is stable, whereas for $\kappa_r > 0$ and $Q > 0$, TwR is stable.

More interesting dynamics can be obtained for $\kappa_r Q < 0$. It is obvious from Table II that no stable patterns are possible in this case. Therefore, nontrivial dynamics, such as the emergence of a heteroclinic cycle is expected. Analyzing the last column of Table II, we conclude that for $\kappa_r < 0$ and $Q > 0$ the heteroclinic connection AR$\rightarrow$ WR2 $\rightarrow$ TwR $\rightarrow$ AR is possible. The sketch of this heteroclinic connection is presented in Fig. 6. Indeed, it is clear from Table II that the unstable manifold of ARs, $\Delta = \pi$, coincides with the stable manifold of WR2. Then, the unstable manifold of WR2 is $\Phi = -\Psi = \Phi_0$, which is the stable manifold of TwR. Finally, $\Delta = 0$ materializes both the unstable manifold of TwR and the stable manifold of ARs. Thus, for this loop a stable manifold of each point coincides with the unstable manifold of the previous point and the necessary stability condition is valid for this heteroclinic cycle [18]. Of course, each AR pattern, either AR-A, or AR-B, or AR-C, forms its own heteroclinic cycle, but following Ref. [19] we treat the group orbit of these heteroclinic connections as a single heteroclinic cycle.

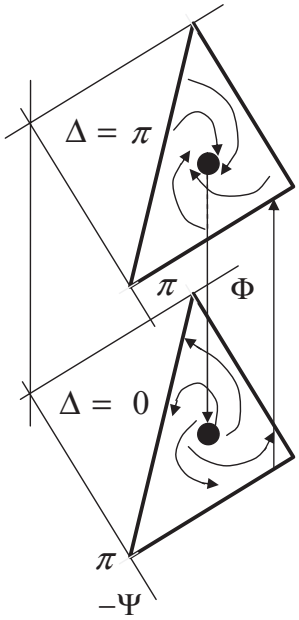


FIG. 6. Scheme of the heteroclinic connection. Condition (43) is met inside the triangles. Solid thick lines (sides of the triangles) correspond to ARs, the lower central point to TwR, the upper one to WR2.

It is possible to apply the sufficient condition of the stability of a heteroclinic cycle [20], calculating the product of the real parts of the positive (unstable) eigenvalues over all saddle points of the heteroclinic cycle and the similar product of the leading negative (stable) eigenvalues. It is clear from Table II that these two products are equal to each other, that is, the system is exactly at the stability border and a more delicate analysis is needed. In particular, this coincidence means that a conventional superexponential growth or decay of perturbations with the number of the cycle does not take place in our case.

A separate analysis of the opposite case $\kappa_r > 0$ and $Q < 0$ is not necessary here, as a change of the sign in $\kappa$, and, hence, due to Eq. (54) in $Q$, is equivalent to inversion of time $\tau_2$ in the set of Eqs. (53). Therefore, the heteroclinic connection AR$\rightarrow$ TwR $\rightarrow$ WR2 $\rightarrow$ AR emerges in this case and the criterion formulated by Melbourne *et al.* [20] does not determine whether the cycle is stable or not.

Numerical calculations show that for the problem considered here $\kappa_r < 0$ in the entire domain of parameters, whereas $Q$ changes its sign. Therefore for the oscillatory Marangoni convection two possibilities exist: for $Q < 0$, WR2 is the only stable pattern attained independently of the initial conditions. In the opposite case, $Q > 0$, all limit cycles are supercritical and unstable. The latter situation is studied below in detail.

The domains of a fixed sign for $Q$ are shown in Fig. 7, where $Sc = P/L$ is the Schmidt number. One can see that for small $|\chi|$ (domain 2), WR2 are stable, whereas for larger $|\chi|$ (domain 1), a heteroclinic cycle emerges.

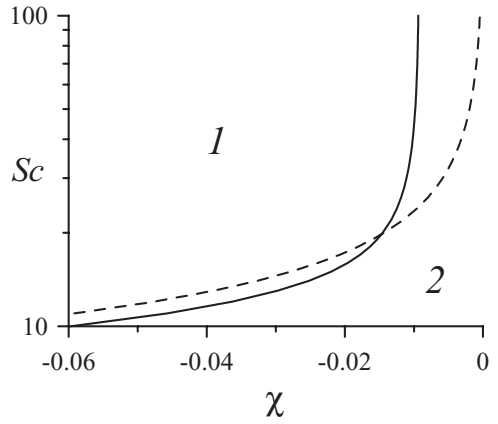


FIG. 7. Stability boundaries $Sc = P/L$ vs $\chi$ for $L = 0.01$ (solid line) and $L = 10^{-5}$ (dashed line). Domains 1 and 2 correspond to $Q > 0$, that is, where no stable limit cycles exist, and $Q < 0$, that is, where WR2 are stable, respectively.

## V. ALTERNATING ROLLS

### A. Governing equations

It has been stated above that Eqs. (53) become invalid when one among the amplitudes is small. Consider in more detail, for instance, a pattern close to AR-A, assuming a small $a$. This analysis is needed only for $Q\kappa_r < 0$, when the heteroclinic cycle emerges. In this case, all ARs represent saddle points, that is, the system approaches AR along its stable manifold and then leaves this fixed point along the unstable manifold. To construct a map valid in the small vicinity of AR, we limit ourselves by $Q > 0$ and $\kappa_r < 0$. Thus, the stable and unstable manifolds are $\Delta = 0$ and $\Delta = \pi$, respectively.

As Eqs. (53c), (56), and (57) are valid, the evolution along the stable manifold is described by

$$a^2 = a_-^2 \exp\left[\tfrac{1}{2}\kappa_r(\tau_2 - \tau_-)\right], \tag{63a}$$
$$\Delta = \Delta_- \exp[-Q(\tau_2 - \tau_-)], \tag{63b}$$
$$\Phi = \tfrac{1}{2}\kappa_i(\tau_2 - \tau_-) + \Phi_-, \tag{63c}$$

whereas along the unstable manifold we obtain

$$a^2 = a_+^2 \exp\left[-\tfrac{3}{2}\kappa_r(\tau_2 - \tau_+)\right], \tag{64a}$$
$$\Delta = \pi + \Delta_+ \exp[Q(\tau_2 - \tau_+)], \tag{64b}$$
$$\Phi = -\tfrac{3}{2}\kappa_i(\tau_2 - \tau_+) + \Phi_+. \tag{64c}$$

Here $a_\pm$ are sufficiently small in order to ensure that the linearized version of Eqs. (53) is valid. (Recall that $\Psi \approx \Phi - \pi$ for AR-A.)

Our purpose is to construct the mapping

$$\{a_-, \Delta_-, \Phi_-\} \to \{a_+, \Delta_+, \Phi_+\}.$$

Indeed, a decay described by Eqs. (63) cannot lead to $a = 0$. When $a$ becomes of order $\delta$, that is, the contribution of waves $A_j$ to $h$ is $O(\delta^2)$ [cf. Eq. (20)], cubic with respect to $A_j$ terms become $O(\delta^6)$, that is, they govern the dynamics of $A_j$ in $\tau_2$ (not in $\tau_1$!). On the other hand, all the quintic terms involving products of at least two $A_j$ have to be omitted. In other words, $\dot{A}_j$ is governed by $b^4 A_j$, $c^4 A_j$, and $a^2 A_j$ instead of $a^4 A_j$.

Therefore we need to reproduce the analysis of Eqs. (29) and (48) for the patterns close to AR-A starting from "large" amplitudes $B_j^{(1)}$ and $C_j^{(1)}$. It is readily seen that

$$\dot{\Phi} - \dot{\Psi} = \dot{b} = \dot{c} = 0, \tag{65}$$

that is, $b^2 = c^2 = 1/2$ and $\Phi - \Psi = \pi$. Moreover, the phases of these four waves evolve according to the law

$$\dot{\phi}_{B1} = \dot{\phi}_{B2} = \dot{\phi}_{C1} = \dot{\phi}_{C2} = -\omega_2 \equiv \frac{1}{4}\left(\kappa_i - \frac{K_{1i}}{K_{1r}}\kappa_r\right), \tag{66}$$

that is, all "large" complex amplitudes oscillate in slow time with the same frequency $\omega_2$. By an appropriate choice of the origin it is possible to set

$$\phi_{B1} = \phi_{B2} = \phi_{C1} - \frac{\pi}{2} = \phi_{C2} - \frac{\pi}{2}, \tag{67}$$

and this is assumed hereafter throughout Sec. V.

In order to describe the "small" waves we introduce rescaled amplitudes $\tilde{A}_j = \delta^{-1} A_j \exp(i\omega_1\tau_1 + i\omega_2\tau_2)$ and by combining Eqs. (29) and (48) obtain

$$\dot{\tilde{A}}_1 = -\frac{\kappa}{4}(\tilde{A}_1 + 2\tilde{A}_2) + \sigma(|\tilde{A}_2|^2 - |\tilde{A}_1|^2)\tilde{A}_1, \tag{68a}$$
$$\dot{\tilde{A}}_2 = -\frac{\kappa}{4}(\tilde{A}_2 + 2\tilde{A}_1) + \sigma(|\tilde{A}_1|^2 - |\tilde{A}_2|^2)\tilde{A}_2. \tag{68b}$$

Introducing phases and real amplitudes by $\tilde{A}_j = \tilde{a}_j \exp(i\tilde{\phi}_{Aj})$, we obtain

$$\dot{p} = -\frac{1}{2}\kappa_r p - 4\sigma_r q^2 + \kappa_r\sqrt{p^2 - q^2}\cos\Delta, \tag{69a}$$
$$\dot{q} = -\frac{1}{2}\kappa_r q - 4\sigma_r pq + \kappa_i\sqrt{p^2 - q^2}\sin\Delta, \tag{69b}$$
$$\dot{\Delta} = -4\sigma_i q - \frac{\kappa_i q\cos\Delta + \kappa_r p\sin\Delta}{\sqrt{p^2 - q^2}}, \tag{69c}$$
$$\dot{\mu} = -\frac{1}{2}\kappa_i + \frac{\kappa_i p\cos\Delta + \kappa_r q\sin\Delta}{\sqrt{p^2 - q^2}}, \tag{69d}$$

where

$$p = \tfrac{1}{2}(\tilde{a}_1^2 + \tilde{a}_2^2), \quad q = \tfrac{1}{2}(\tilde{a}_1^2 - \tilde{a}_2^2), \tag{70a}$$
$$\mu = \tilde{\phi}_{A1} + \tilde{\phi}_{A2}. \tag{70b}$$

It is noteworthy that based on Eq. (67) and on the relation between the phases of $A_j$ and $\tilde{A}_j$, it is possible to conclude that $\Delta = \tilde{\phi}_{A1} - \tilde{\phi}_{A2}$, whereas $\mu = \Phi$ up to unimportant additive constants. Below, we consider $\Phi_+ - \Phi_-$ as a gain in $\mu$ during the stage when the system is close to AR.

### B. Splitting of Eqs. (69)

Solution of Eqs. (68) or (69) can be split into solution of several matched linear problems as sketched in Fig. 8. We briefly discuss here only the differential equations governing the dynamics of the system and their solutions, whereas the matching procedure will be presented in Sec. V C.

During stage I

$$p \gg 1, \quad |q| \ll 1, \quad \Delta = \Delta_0 + \Delta_1, \tag{71}$$

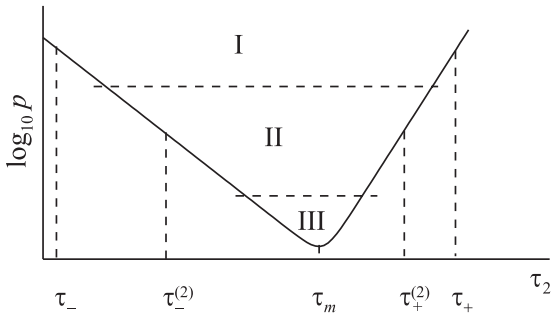


FIG. 8. A scheme of splitting of Eqs. (68) [Eqs. (69)]. The set of Eqs. (72) is valid at stage I, Eqs. (72a), (72b), and (75) are valid at stage II. A linearized set of Eqs. (77) is appropriate at stage III.

where $\Delta_0 = 0$ for the decaying tail, $\Delta_0 = \pi$ for the growing one, and $|\Delta_1| \ll 1$. Thus, at the leading order Eqs. (69) can be rewritten as

$$\dot{p} = \frac{\kappa_r}{2}(2\cos\Delta_0 - 1)p, \tag{72a}$$

$$\dot{\mu} = \frac{\kappa_i}{2}(2\cos\Delta_0 - 1), \tag{72b}$$

$$\dot{q} = (-4\sigma_r q + \kappa_i \cos\Delta_0\Delta_1)p, \tag{72c}$$

$$\dot{\Delta}_1 = -4\sigma_i q - \kappa_r \cos\Delta_0\Delta_1, \tag{72d}$$

and the corresponding solution is

$$p = p_\pm \exp\left[\frac{\kappa_r}{2}(2\cos\Delta_0 - 1)(\tau_2 - \tau_\pm^{(1)})\right], \tag{73a}$$

$$\mu = \frac{\kappa_i}{2}(2\cos\Delta_0 - 1)(\tau_2 - \tau_\pm^{(1)}) + \mu_\pm, \tag{73b}$$

$$q = \frac{\kappa_i}{4\sigma_r}\cos\Delta_0\Delta_1 + O(p^{-1}), \tag{73c}$$

$$\Delta_1 = \Delta_\pm^{(1)} \exp[\mp Q(\tau_2 - \tau_\pm^{(1)})]. \tag{73d}$$

Note that we neglect the term $\dot{q}$ in Eq. (72c), which hence is reduced to the linear *algebraic* equation. This means that "fast" relaxation (on the time scale, proportional to $p^{-1}$) of $q$ to the solution, given by Eq. (73c), is omitted.

During the next stage of evolution, stage II, $p$ is finite, while $q$ and $\Delta_1$ are still small. Thus, Eqs. (72a) and (72b) and their solutions Eqs. (73a) and (73b) remain valid. It is convenient to rewrite the former solution as

$$p = \exp\left[\frac{\kappa_r}{2}(2\cos\Delta_0 - 1)(\tau_2 - \tau_\mp^{(2)})\right] \tag{74}$$

at the decaying and growing tails, respectively. Here $\tau_-^{(2)} \equiv \tau_-^{(1)} - 2\kappa_r^{-1}\ln p_-$ and $\tau_+^{(2)} \equiv \tau_+^{(1)} + 2(3\kappa_r)^{-1}\ln p_+$.

The coupled dynamics of $q$ and $\Delta_1$ is governed by

$$\dot{q} = -\frac{\kappa_r}{2}q - (4\sigma_r q - \kappa_i \cos\Delta_0\Delta_1)p, \tag{75a}$$

$$\dot{\Delta}_1 = -4\sigma_i q - \cos\Delta_0(\kappa_r\Delta_1 + \kappa_i p^{-1}q), \tag{75b}$$

Equations (75) represent a linear set with variable coefficients which will be solved numerically. An analytical solution is possible only in one of two limiting cases: when $p \gg 1$ ($\tau_2 \ll \tau_-^{(2)}$ or $\tau_2 \gg \tau_+^{(2)}$) and when $p \ll 1$ ($\tau_2 \gg \tau_-^{(2)}$ or $\tau_2 \ll \tau_+^{(2)}$). (In fact, due to the exponential dependence on $\tau_2 - \tau_\pm^{(2)}$, the time difference can be finite but sufficiently large.) In the former case, the solutions are given by Eqs. (73c) and (73d), see details of matching below. In the latter case, the solution of Eqs. (75) is

$$\Delta = \Delta_0 + b_\pm \exp[\pm\kappa_r(\tau_2 - \tau_\pm^{(2)})]\sin\phi_\pm, \tag{76a}$$

$$q = b_\pm \exp\left[-\frac{\kappa_r}{2}(\tau_2 - \tau_\pm^{(2)})\right]\cos\phi_\pm,$$
$$\phi_\pm = \alpha_\pm \pm \kappa_i(\tau_2 - \tau_\pm^{(2)}), \tag{76b}$$

so that at the boundary between stages II and III, that is, at $\tau_2 \gg \tau_-^{(2)}$ on the decaying tail and at $\tau_2 \ll \tau_+^{(2)}$ on the growing tail, the amplitudes $\tilde{a}_j$ become small. Thus, at stage III Eqs. (68) can be linearized to yield

$$\dot{\tilde{A}}_1 = -\frac{\kappa}{4}(\tilde{A}_1 + 2\tilde{A}_2), \tag{77a}$$

$$\dot{\tilde{A}}_2 = -\frac{\kappa}{4}(\tilde{A}_2 + 2\tilde{A}_1). \tag{77b}$$

The solution of this set of equations reads

$$\tilde{A}_{1,2} = \tilde{D}_1 e^{\kappa(\tau_2 - \tau_m)/4} \pm \tilde{D}_2 e^{-3\kappa(\tau_2 - \tau_m)/4}. \tag{78}$$

with arbitrary complex constants $\tilde{D}_1$ and $\tilde{D}_2$. Note that it is convenient to define $\tau_m$ so that $|\tilde{D}_1| = |\tilde{D}_2|$.

### C. Details of the matching procedure

We now describe the matching procedure for the above mentioned solutions in order to construct the local map.

Along the decaying tail, at $\tau_- < \tau_2 < \tau_-^{(1)}$, Eqs. (73) agrees with the "external solutions" given by Eqs. (63). Matching these solutions, we obtain

$$p_- = \frac{a_-^2}{\delta^2}\exp\left[\frac{\kappa_r}{2}(\tau_-^{(1)} - \tau_-)\right], \tag{79a}$$

$$\mu_- = \Phi_- + \frac{\kappa_i}{2}(\tau_-^{(1)} - \tau_-), \tag{79b}$$

$$\Delta_-^{(1)} = \Delta_- \exp[-Q(\tau_-^{(1)} - \tau_-)]. \tag{79c}$$

The first relation provides that the duration of stage I along the decaying tail $\tau_-^{(1)} - \tau_-$ is proportional to $\ln\delta$. The small matching value $a_-$ has to be chosen in such way that $a_- \gg \delta$ in order to ensure a large value of $p_-$. Furthermore, $\Delta_1$ is rather small, as it decays exponentially during this stage. Indeed,

$$\Delta_-^{(1)} = \Delta_-\left(\frac{p_-\delta^2}{a_-^2}\right)^{-2Q/\kappa_r} \ll 1,$$

therefore assumptions given by Eq. (71) are satisfied by the matching procedure.

Thus, stage I provides the matching of Eqs. (53) and (68). During this stage $p$ decays and grows according to the linearized version of Eqs. (53), and this stage lasts the time interval proportional to $\ln\delta$ in order to ensure the decay and growth of the amplitude by the factor $\delta$.

As we noted in Sec. V B, during stage II the evolution of $p$ and $\mu$ is still governed by Eqs. (73a) and (73b), respectively. Hence, at the beginning of stage II, $p$ is sufficiently large, that is, the solutions for $q$ and $\Delta_1$ given by Eqs. (73c) and (73d) are valid. This provides initial conditions for Eqs. (75) with $\Delta_0 = 0$.

Numerical solution of Eqs. (75) for $\Delta_0 = 0$ with given asymptotics for $\Delta_1$ and $q$ at $\tau_2 \ll \tau_-^{(2)}$ allows us to calculate the constants $b_-$ and $\alpha_-$, which enter into Eqs. (76), that is, the solution in the opposite limiting case $\tau_2 \gg \tau_-^{(2)}$. Note that $b_- \sim \Delta_-^{(1)}$, that is, one can set $b_- = \Delta_-^{(1)}\tilde{b}_-$, where $\tilde{b}_-$ is independent of $\delta$ together with $\alpha_-$.

In order to ensure the matching of solutions at stages II and III, Eqs. (76) and (78), respectively, we calculate $\Delta = \arg(\tilde{A}_1/\tilde{A}_2)$ and $q = \frac{1}{2}(|\tilde{A}_1|^2 - |\tilde{A}_2|^2)$ at $\tau \ll \tau_m$. This leads to

$$\Delta \approx 2\exp[-\kappa_r(\tau_2 - \tau_m)]\sin\beta_\alpha, \tag{80a}$$

$$q \approx 2d_l^2 \exp\left[-\frac{\kappa_r}{2}(\tau_2 - \tau_m)\right]\cos\beta_\alpha, \tag{80b}$$

where $\beta_\alpha = \beta_2 - \beta_1 - \kappa_i(\tau_2 - \tau_m)$ and $\tilde{D}_j = d_l\exp(i\beta_j)$. (Recall that $|\tilde{D}_1| = |\tilde{D}_2| \equiv d_l$.) Therefore, matching of solutions at stages II and III allows us to calculate the complex amplitudes $\tilde{D}_1$ and $\tilde{D}_2$:

$$d_l^4 = \frac{b_-}{2}, \quad \beta_1 = \frac{\kappa_i}{4}(\tau_m - \tau_-), \tag{81a}$$

$$\beta_2 = \beta_1 - \kappa_i(\tau_m - \tau_-^{(2)}) + \alpha_-. \tag{81b}$$

With an increase in $\tau_2$, the second term in Eq. (78) becomes dominant. It follows that $\tilde{A}_1 \approx -\tilde{A}_2$, and thus $\Delta$ is close to $\pi$ at $\tau_2 \gg \tau_m$. Therefore following stage III, Eqs. (75) becomes valid again, but with $\Delta_0 = \pi$. It is obvious that $p$, which is given by both Eqs. (73a) and (74), can be represented by

$$p = d_l^2 \exp\left[-\tfrac{3}{2}\kappa_r(\tau - \tau_m)\right]. \tag{82}$$

Moreover, the phase $\mu$ can be easily calculated based on Eq. (78):

$$\mu \approx \arg\left(-\tilde{D}_2^2 e^{-3\kappa(\tau_2-\tau_m)/2}\right) = \pi + 2\beta_2 - \tfrac{3}{2}\kappa_i(\tau_2 - \tau_m). \tag{83}$$

These representations for $p$ and $\mu$ can be matched with Eqs. (73a) and (73b) at stage I which results in

$$p_+ = d_l^2 \exp\left[-\tfrac{3}{2}\kappa_r(\tau_+^{(1)} - \tau_m)\right], \tag{84a}$$

$$\mu_+ = \pi + 2\beta_2 - \tfrac{3}{2}\kappa_i(\tau_+^{(1)} - \tau_m). \tag{84b}$$

Then, matching Eq. (78) with Eqs. (76) enables us to determine the constants $b_+$ and $\alpha_+$:

$$b_+ = (4b_-)^{1/3}, \quad \alpha_+ = \kappa_i(\tau_+^{(2)} - \tau_-^{(2)}) - \alpha_-. \tag{85}$$

Numerical solution of Eqs. (75) with $\Delta_0 = \pi$ transforms the initial data $b_+$,$\alpha_+$ at $\tau_2 \ll \tau_+^{(2)}$ to the constant $\Delta_+^{(1)}$ appearing in Eqs. (73c) and (73d). Obviously that $\Delta_+^{(1)} = \Delta_\infty b_+ \sim [\Delta_-^{(1)}]^{1/3}$. The coefficient $\Delta_\infty$ must be found numerically for any given value of $\alpha_+$.

Finally, the solution at stage I given by Eqs. (73) must be connected with the solution of the external problem [Eqs. (64)]. This procedure yields

$$a_+^2 = p_+\delta^2 \exp\left[-\tfrac{3}{2}\kappa_r(\tau_+ - \tau_+^{(1)})\right], \tag{86a}$$

$$\Phi_+ = \mu_+ - \tfrac{3}{2}\kappa_i(\tau_+ - \tau_+^{(1)}), \tag{86b}$$

$$\Delta_+ = \Delta_+^{(1)}\exp[Q(\tau_+ - \tau_+^{(1)})], \tag{86c}$$

and again the duration of stage I is proportional to $\ln\delta$.

Summarizing all the connections mentioned above and setting hereafter $a_+ = a_-$, we conclude that

$$\Delta_+ = \Delta_\infty(4\Delta_-\tilde{b}_-)^{1/3}, \tag{87a}$$

$$\Phi_+ = \Phi_- + \pi + 2\alpha_- + \frac{1}{2}\kappa_i(\tau_-^{(2)} - \tau_-) - \frac{3}{2}\kappa_i(\tau_+ - \tau_-^{(2)}), \tag{87b}$$

$$\tau_+ = \tau_- + \frac{1}{3\kappa_r}\ln\left[\frac{\Delta_-\tilde{b}_-}{2}\left(\frac{\delta}{a_-}\right)^{4(1-Q/\kappa_r)}\right], \tag{87c}$$

$$\tau_-^{(2)} = \tau_- + \frac{1}{\kappa_r}\ln\frac{\delta}{a_-}, \tag{87d}$$

$$\tau_+^{(2)} = \tau_+ - \frac{1}{3\kappa_r}\ln\frac{\delta}{a_-}. \tag{87e}$$

Here, as stated above, three out of the constants $\Delta_\infty$, $\tilde{b}_-$, and $\alpha_-$ are determined from numerical solution of Eqs. (75) with either $\Delta_0 = \pi$ or $\Delta_0 = 0$. Recall that $\Delta_\infty$ depends on $\alpha_+$ and, hence, due to Eqs. (85) and (87), on $\ln\delta$ and $\Phi_-$.

It is important for the further analysis that

$$\Delta_+ = \eta\Delta_-^{1/3}, \tag{88}$$

where

$$\eta \equiv \Delta_\infty(4\tilde{b}_-)^{1/3}.$$

Another important feature of the system under consideration is the gain in $\Phi$, $\Phi_+ - \Phi_-$, and duration of a near-AR stage $\tau_+ - \tau_-$ depending on $\ln\delta$. To reiterate, $\delta$ is an asymptotically small parameter, but its logarithm is retained in the analysis. The dependence of $\Phi_+ - \Phi_-$ on the logarithm of supercriticality is a direct consequence of linear variation of the phase $\mu$ along both the decaying and the growing tails, which endure almost the entire period $\tau_+ - \tau_-$.

Let us now discuss the choice of numerical constants which appear in Eqs. (87). Recall that one has to set $a_-$ to be rather small in order to justify linearization of Eqs. (53) with respect to small $a^2$. Strictly speaking we do not need the value of $\delta$, only $\ln\delta$ is present in the local map [Eqs. (87)]. However, we set $\delta$ to be sufficiently small in order to ensure that $p_\pm = a_-^2\delta^{-2}$ is large.

Numerical solution of Eqs. (69) with a sufficiently large initial value of $p$ agrees well with the solution of the above-mentioned sequence of linearized problems [Eqs. (72), (75), and (77)]. An example of such solution is given in Fig. 9 where all five stages are clearly seen: exponential decay of $\Delta$, $q$, and $p$ with an almost linear variation of $\Phi$.

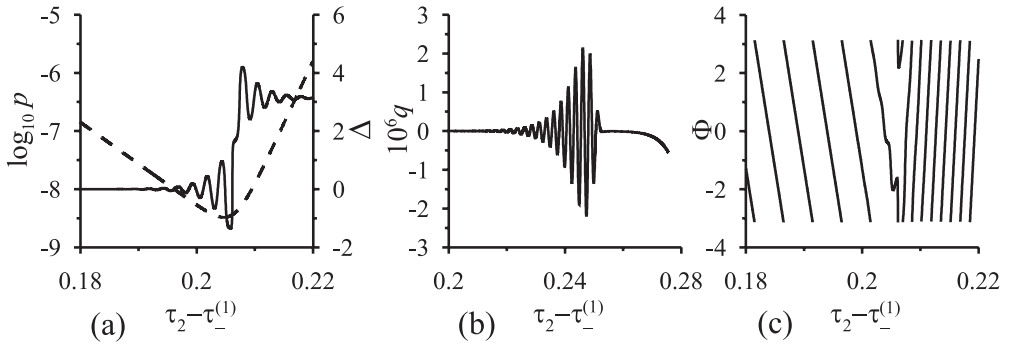


FIG. 9. Solution of Eqs. (69) for $\chi = -0.05$, $L = 0.01$, $Sc = 200$. (a) Variation of $\log_{10} p$ (dashed line) and $\Delta$ (solid line) with time $\tau_2$. (b) Variation of $q(\tau_2)$. (c) $\Phi(\tau_2)$. Initial conditions at $\tau = \tau_-^{(1)}$ are $p = 10^6$, $\Delta = 8.62 \times 10^{-2}$, $\Phi = 0$.

Then, both $\Delta$ and $q$ start growing at stage II; after that the linearized equations for the amplitudes $\tilde{A}_j$ become valid at stage III which leads to $\Delta \approx \pi$. Finally, the amplitude of the "reflected" wave starts to grow. During stage II this process is accompanied by an initial increase in $q$, then $q$ tends to zero, and finally it grows proportionally to $\Delta_1$ at stage I.

It is important to emphasize that contrary to the above-mentioned equivalence of a change of sign in $\kappa$ and the time inversion in Eqs. (53), the entire coupled set of Eqs. (53) and (68) changes under simultaneous substitution $\kappa \to -\kappa$, $\tau_2 \to -\tau_2$. Therefore, the case $\kappa_r > 0$, $Q < 0$ should be treated separately. We do not present the analysis here, and results are very similar to those for $\kappa_r < 0$, $Q > 0$. Note that $\kappa_r < 0$ for the Marangoni convection.

## VI. RESULTS

### A. Numerical results

Numerical solution of the sets of Eqs. (53) and (68) demonstrates the emergence of the heteroclinic cycle. A typical elementary loop of this evolution, WR2 → TwR → AR → WR2, is presented in Fig. 10. One can see that the system visits all three unstable fixed points, being alternately attracted to and

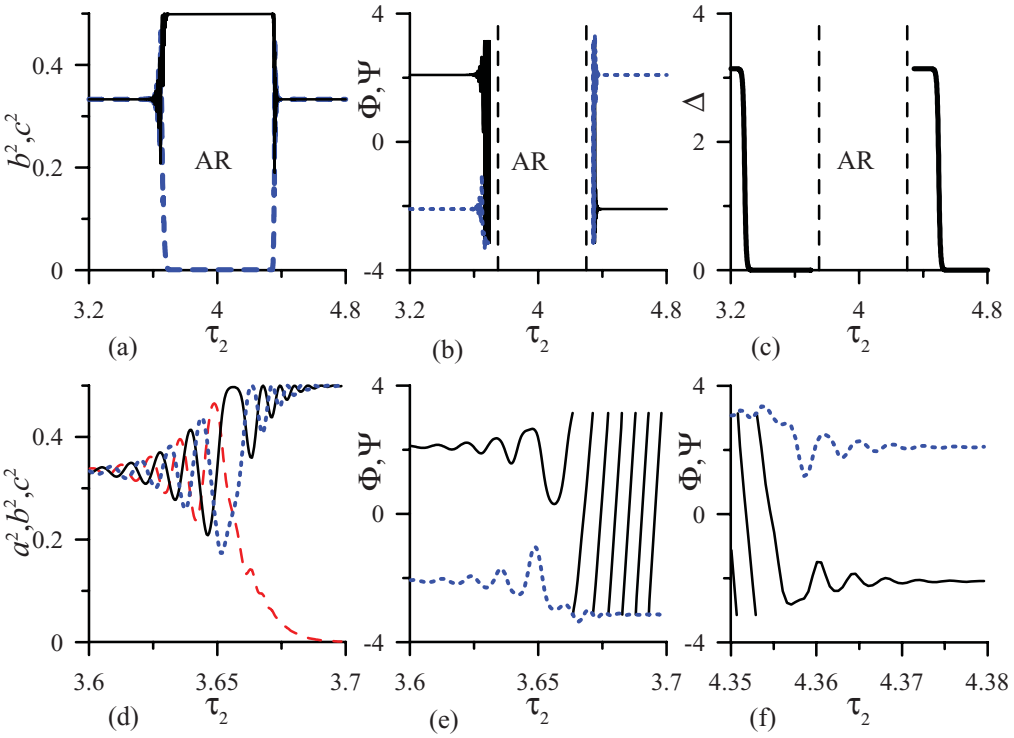


FIG. 10. (Color online) Example of evolution within a single loop of the heteroclinic connection for $\chi = -0.05$, $L = 0.01$, $Sc = 200$. During the period marked with "AR" the system evolves according to Eqs. (69), see Fig. 9. (a) Dashed and solid lines correspond to $b^2(\tau_2)$ and $c^2(\tau_2)$, respectively; (b) $\Phi(\tau_2)$ and $\Psi(\tau_2)$ shown by the solid and dashed lines, respectively; and (c) $\Delta(\tau_2)$. Details of the evolution near AR-B are shown in panels (d)–(f): (d) the squared amplitudes $a^2$, $b^2$, and $c^2$ shown by the dotted, dashed, and solid lines, respectively; (e) and (f) phase differences $\Phi$ and $\Psi$ shown by the solid and dotted lines, respectively.

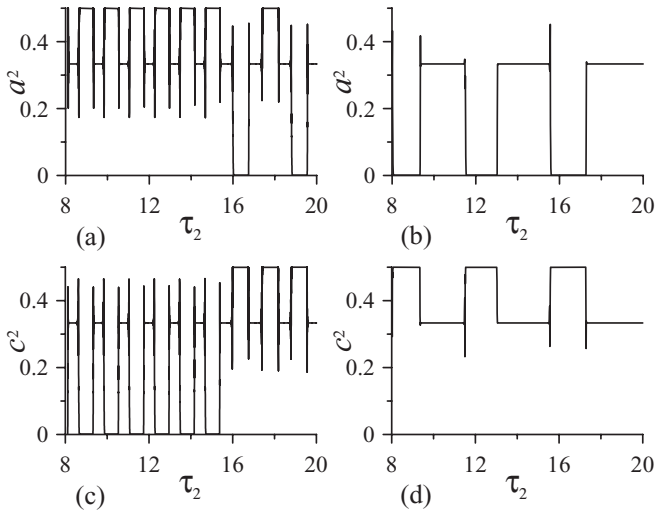


FIG. 11. Evolution of the squared amplitudes in slow time $\tau_2$ for $\chi = -0.05$, $L = 0.01$, $Sc = 200$: (a) and (b) $a^2(\tau_2)$; (c) and (d) $c^2(\tau_2)$. (a) and (c) direct numerical solution of Eqs. (53) (set 1), (b) and (d) solution in terms of new variables $\xi$ and $\nu$, Eqs. (89) and (90) (set 2).

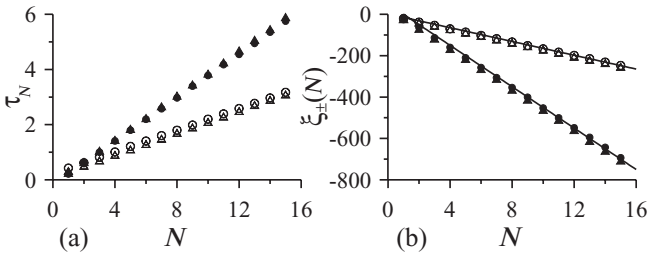


FIG. 12. Characteristics of the $N$th cycle for $\chi = -0.05$, $L = 0.01$, $Sc = 200$. Circles and triangles correspond to $\delta = 10^{-6}$ and $\delta = 10^{-4}$, respectively. (a) Duration of an AR state $\tau_+(N) - \tau_-(N)$ (open symbols) and symmetric AH $\tau_+^{(s)}(N) - \tau_-^{(s)}(N)$ (filled symbols) depending on $N$. (b) Representation $\xi_-(N)$ (filled symbols) and $\xi_+(N)$ (open symbols). The lines depict the asymptotic expression corresponding to the global map given by Eq. (103).

then repelled from each of them. Starting from a pattern close to WR2 at $\tau_2 = 3.2$ the system suddenly approaches TwR [see decrease in $\Delta$ in Fig. 10(c)]. Then, the differences in the amplitudes $a^2$, $b^2$, and $c^2$ start to grow [see Figs. 10(a) and 10(d)] which is accompanied by an almost linear evolution of $\Phi$ at $\Psi \approx -\pi$ shown in Fig. 10(e). Therefore, the pattern is close to AR-B at this stage and the phases $\Phi$, $\Delta$, and the smallest amplitude $b^2$ evolve as it has been described in Sec. V. At the final step of this stage, again, $\Phi$ changes almost linearly [Fig. 10(f)], whereas $\Delta$ is close to $\pi$. Then, $b^2$ starts to grow and at $\tau_2 \approx 4.37$, WR2 is approached: $a^2 \approx b^2 \approx c^2$ ($\Psi = -\Phi = 2\pi/3$) and $\Delta \approx \pi$. After that the cycle is repeated.

However, such evolution does not form a regular cycle due to two reasons: first, any AR pattern among the three (AR-A, AR-B, or AR-C) can be reached at the current loop. Second, several saddle points, all ARs and WR2, are the saddle-foci, that is, the details of the attraction to these points are different from one cycle to another.

Moreover, the observed dynamics at large times strongly depends on the accuracy of computations. To demonstrate this fact we introduce a new variable $\xi \equiv \ln|\tan(\Delta/2)|$, which transforms Eq. (53c) into

$$\dot{\xi} = -2Q(a^4 + b^4 + c^4). \tag{89}$$

Also, close to a symmetric AH, an auxiliary complex variable $\nu \equiv \ln\zeta$ is introduced, where $\zeta \equiv \Phi - \Phi_0 + e^{i2\pi/3}(\Psi + \Phi_0)$. It allows us to rewrite Eqs. (53a) and (53b) as

$$\dot{\nu} = \tfrac{2}{9}\kappa(1 + 2\tanh\xi). \tag{90}$$

The system is interpreted to be close to a symmetric AH at $\tau_-^{(s)} < \tau_2 < \tau_+^{(s)}$, when $|\zeta| < \varepsilon$. (In the computations we choose $\varepsilon = 10^{-6}$.) Otherwise, Eqs. (53a) and (53b) are solved together with Eq. (89). An introduction of $\xi$ and $\nu$ considerably increases the accuracy of computations. Indeed, an exponential decay of $\Delta$ (or $\pi - \Delta$) and $\Phi - \Phi_0$, $\Psi + \Phi_0$ with $\tau_2$ corresponds to the linear variation of $\xi$ and $\nu$, respectively.

In order to demonstrate the efficiency of these auxiliary variables, we perform two types of computations. First, we solve directly Eqs. (53) and (68) in terms of the phases, $\Phi$, $\Psi$, and $\Delta$ referred to as set 1. Then, as set 2, we use auxiliary variables $\xi$ and $\nu$ solving Eq. (89) instead of Eq. (53c) and for $\tau_-^{(s)} < \tau_2 < \tau_+^{(s)}$ Eq. (90) instead of Eqs. (53a) and (53b). The results of the numerical computations are presented in Figs. 11(a) and 11(c) for set 1 and in Figs. 11(b) and 11(d) for set 2. The same initial conditions were chosen for these two solutions, but the evolution is found to be close only during the first loop. One can readily see that for set 1 any AR with either $a = 0$, or $b = 0$, or $c = 0$ can be reached randomly at the current cycle. For set 2, at large $\tau_2$ only one of AR is possible. For instance, under initial conditions chosen in Fig. 11(b) AR-A is found, that is, $a = 0$. Another important feature is that duration of each cycle is almost constant in set 1 and grows in set 2. The duration of stay in a close vicinity of one of the unstable fixed points $\tau_N$ increases with the cycle number $N$ almost linearly [see Fig. 12(a)]. Note that no conventional exponential growth of the period is found, because we are exactly at the stability boundary according to the criterion of Melbourne *et al.* [20].

Thus, the time period for set 1 observed in Figs. 11(a) and 11(c) is determined by the level of numerical noise during the calculations [21,22]. However, increasing the tolerance of computations we are not able to considerably change this period. To demonstrate this fact, we use the representation $\xi_\pm(N) \equiv \mp\xi\,(\tau_\pm)$ in Fig. 12(b). As clearly seen from this figure, $\Delta$ becomes very small (or close to $\pi$) during several cycles and no numerical method is able to capture such a small value. This decrease in $\xi_\pm(N)$, as well as the increase in $\tau_N$, shows that the vector flow corresponding to Eqs. (53) and (68) is contracting in the vicinity of the heteroclinic cycle. Therefore, being both important, sets 1 and 2 correspond to different physical situations. Set 1 predicts the behavior which can be found in real or numerical experiments, whereas set 2 clearly indicates a stability of the heteroclinic cycle within an idealized noise-free system.

Variation of $\delta$ does not change the dynamics qualitatively, see Fig. 12; the linear dependencies of $\tau_N$ and $\xi_\pm(N)$ on $N$ remain almost the same, while $\delta$ increases by two orders

of magnitude. However, each loop of evolution drastically changes with a decrease in $\delta$. For instance, the duration of the cycle increases. Similar variation was found when $a_-$ changes.

### B. Global map for the heteroclinic cycle

Numerical results described in Sec. VI A show that the heteroclinic cycle is stable. In order to demonstrate that the heteroclinic connection is attracting, we will construct the global map for the cycle.

We start with near-AR evolution, when the local map, given by Eq. (88), can be applied. Starting with $a = a_-$ and $\Delta = \Delta_-^{(n)}$ for $\tau_2 = \tau_-$, we obtain $a = a_-$ and $\Delta = \Delta_+^{(n)}$ for $\tau_2 = \tau_+$. Here the superscript $(n)$ indicates the $n$th loop along the heteroclinic connection. In what follows we omit the superscript where that does not lead to misunderstanding.

The trajectory leaves the vicinity of AR-A and approaches WR2. With increase in $a$ Eqs. (53) valid in the general case are solved. However, during this stage, AR-A→WR2, $\Delta$ is still close to $\pi$, which allows us to rewrite these equations as follows:

$$\dot{\Phi} = 6c^2 \mathrm{Im}(Fe^{-i\Psi}), \tag{91a}$$

$$\dot{\Psi} = -6b^2 \mathrm{Im}(Fe^{-i\Phi}), \tag{91b}$$

$$\partial_{\tau_2} \ln \Delta_1 = 2Q(a^4 + b^4 + c^4), \tag{91c}$$

where, again, $\Delta = \pi + \Delta_1$. Thus the distinction between $\Delta$ and $\pi$ is unimportant for evolution of both $\Phi$ and $\Psi$. Dynamics of these two phases cannot be found analytically, but the phase portrait is determined by

$$\frac{d\Phi}{d\Psi} = -\frac{c^2 \mathrm{Im}(Fe^{-i\Psi})}{b^2 \mathrm{Im}(Fe^{-i\Phi})}. \tag{92}$$

A typical phase portrait on the cross-section $\Delta = \pi$ is shown in Fig. 13. During this stage the remaining phase evolves according to the equation

$$\Delta = \pi - \Delta_+ \exp\left[2Q \int_{\tau_+}^{\tau_2} (a^4 + b^4 + c^4) d\tau_2\right]. \tag{93}$$

The integral in the exponent can be rewritten as

$$\int_{\Phi_+}^{\Phi} G(\Phi) d\Phi, \quad G(\Phi) \equiv \frac{a^4 + b^4 + c^4}{6c^2 \mathrm{Im}(Fe^{-i\Psi})}, \tag{94}$$

where $\Psi$ should be expressed through $\Phi$ via Eq. (92).

This stage lasts until $\tau_2 = \tau_-^{(s)}$, which is determined by the condition $|\zeta(\tau_-^{(s)})| = \varepsilon \ll 1$. [Recall that $\zeta = \Phi - \Phi_0 + e^{i2\pi/3}(\Psi + \Phi_0)$ shows how close is the system to a symmetric pattern with $a = b = c$.] Thus, $\zeta$ becomes small enough and the linearized equations [Eq. (90)] can be applied at the next stage, WR2→TwR. As initial conditions for this stage we use

$$\zeta = \varepsilon e^{i\varphi}, \quad \Delta = \pi + \Delta_w, \tag{95}$$

where

$$\Delta_w \equiv \Delta_+ \exp\left[2Q \int_{\Phi_+}^{\Phi_w} G(\Phi) d\Phi\right] \tag{96}$$

with $\Phi_w \equiv \Phi(\tau_-^{(s)})$.

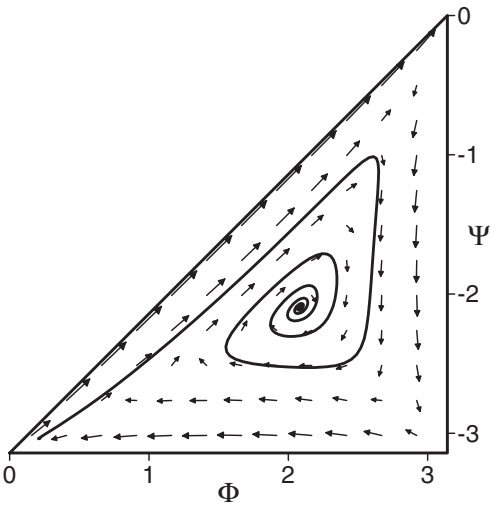


FIG. 13. Vector flow in the plane $\Delta = \pi$, and an example of the phase trajectory. Note that Eq. (61) and its solution Eq. (62) are appropriate near the vertices of the triangle (OHR). Thus the system can approach any of the angles along the stable manifold for OHR, then leaving the vicinity of OHR along its unstable manifold in finite time.

During the transition WR2 → TwR, near-symmetric equations, that is, Eqs. (90) and (89) with $a^2 = b^2 = c^2 = \frac{1}{3}$, are valid. The solution of these equations reads

$$\Delta = 2 \arctan\left\{\frac{2}{\Delta_w} \exp\left[\frac{2}{3} Q(\tau_2 - \tau_-^{(s)})\right]\right\}, \tag{97a}$$

$$\zeta = \varepsilon \exp\left[i\varphi - \frac{2}{9}\kappa(\tau_2 - \tau_-^{(s)})\right] \times \left\{\frac{4 \exp\left[-\frac{4}{3} Q(\tau_2 - \tau_-^{(s)})\right] + \Delta_w^2}{4 + \Delta_w^2}\right\}^{-\frac{2\kappa}{3Q}}. \tag{97b}$$

(Certainly $\Delta_w^2 \ll 4$ and, hence, the second term in the denominator of $\zeta$ can be disregarded.) The system leaves the $\varepsilon$ vicinity of symmetric patterns at $\tau_2 = \tau_+^{(s)}$, when again $|\zeta| = \varepsilon$. It follows that the exponential term is small with respect to $\Delta_w^2$ and

$$\tau_+^{(s)} \approx \tau_-^{(s)} - \frac{6}{Q} \ln \frac{\Delta_w}{2}, \tag{98}$$

$$\Delta \equiv \Delta_t \approx \frac{\Delta_w^3}{4}, \tag{99}$$

that is, $\Delta$ becomes sufficiently small. These formulas serve as the initial conditions for the next stage, namely the transition TwR→AR along the plane $\Delta = 0$. Therefore, we can use equations similar with Eqs. (91) during this stage with obvious changes:

$$\dot{\Phi} = -2c^2 \mathrm{Im}(Fe^{-i\Psi}), \tag{100a}$$

$$\dot{\Psi} = 2b^2 \mathrm{Im}(Fe^{-i\Phi}), \tag{100b}$$

$$\partial_{\tau_2} \ln \Delta = -2Q(a^4 + b^4 + c^4), \tag{100c}$$

and with similar solutions

$$\Delta = \Delta_t \exp\left[6Q \int_{\Phi_t}^{\Phi} G(\Phi) d\Phi\right]. \tag{101}$$

Here again $\Psi$ and $\Phi$ are coupled through Eq. (92). The phase portrait for this stage is similar to that shown in Fig. 13, but with the opposite direction of arrows. At the final state, when one out of the amplitudes $a$, $b$, or $c$ becomes small, we obtain

$$\Delta \equiv \Delta_-^{(n+1)} = \Delta_t \exp\left[6Q\int_{\Phi_t}^{\Phi_-} G(\Phi)d\Phi\right]. \quad (102)$$

(The superscript is used to denote the next loop of the evolution.)

Summarizing Eqs. (88), (96), (99), and (102), we arrive at the global map, which couples $\Delta_-^{(n+1)}$ with $\Delta_-^{(n)}$:

$$\Delta_-^{(n+1)} = \frac{\eta^3}{4}\Delta_-^{(n)}, \quad \Delta_+^{(n+1)} = \frac{\eta}{4^{1/3}}\Delta_+^{(n)}, \quad (103)$$

where the superscripts for $\Delta_\pm^{(n)}$ are restored. Fortunately, the integrals appearing in Eqs. (96) and (102) annihilate each other, under assumption that

$$\int_{\Phi_+}^{\Phi_w} G(\Phi)d\Phi = \int_{\Phi_t}^{\Phi_-} G(\Phi)d\Phi. \quad (104)$$

Indeed, the value of both integrals are determined mainly by slow evolution near the fixed points, corresponding to AR or TwR and WR2; the contribution of the intermediate interval is almost negligible.

Both $\Phi_+$ and $\Phi_-$ are chosen by either the condition $a(\Phi_\pm) = a_-$, or $b(\Phi_\pm) = a_-$, or $c(\Phi_\pm) = a_-$. Therefore, the integration starts from an $a_-^2$ vicinity of one among the ARs. However, as shown in Sec. V, near an AR the system is governed by the smallest squared amplitude, either $a^2$, $b^2$, or $c^2$, rather than by $\Phi$ and $\Psi$. Therefore, the contributions of the vicinities of the points $\Phi_-$ and $\Phi_+$ to the corresponding integral are equal to each other.

Both $\Phi_t$ and $\Phi_w$ are determined by the condition $|\zeta| = \varepsilon$. Again, near the symmetric patterns, $\zeta$ is the appropriate variable and the contributions to the integrals are determined by the initial values of $|\zeta| = \varepsilon$. Therefore, the contributions of the close vicinities of $\Phi_t$ and $\Phi_w$ are equal to each other, and, therefore, Eq. (104) is satisfied.

The global maps for $\Delta_\pm$ [Eq. (103)] are demonstrated in Fig. 12(b) by solid lines. It is clearly seen that the agreement of the numerical results and the analytical formulas [Eq. (103)] is excellent. Our calculations showed that although $\eta$ slightly varies from one cycle to another, it always remains positive and rather small. Therefore, the stability of the heteroclinic cycle is demonstrated both analytically and numerically.

## VII. STABILITY WITH RESPECT TO EXTERNAL PERTURBATIONS

### A. General case analysis

Consider now stability of AH with respect to *external disturbances*, that is, the perturbations which do not belong to the hexagonal lattice. For this purpose, we perturb the base solution $h_0$ given by Eqs. (20) and (41), adding a small-amplitude disturbance $h'$, where

$$h' = \delta(ge^{i\mathbf{k}_p\cdot\mathbf{R}} + de^{-i\mathbf{k}_p\cdot\mathbf{R}})e^{-i\tilde{\Omega}T} + \text{c.c.}, \quad (105a)$$

$$\mathbf{k}_p = k(\cos\phi,\ \sin\phi). \quad (105b)$$

It should be emphasized that we consider the evolution of the external perturbations in $\tau_1$ and, thus, only cubic nonlinear terms are accounted for. We do not consider resonant perturbations, thus setting $\phi \neq n\pi/6$. Indeed, for even $n$ the wave vector belongs to the hexagonal lattice, whereas for odd $n$ a separate analysis is needed (see Sec. VII B).

The evolution of the amplitudes $g(\tau_1)$ and $d(\tau_1)$ is governed by

$$g_{\tau_1} = (\gamma_1 - K_g)g + K_d d^*, \quad (106a)$$

$$d_{\tau_1} = (\gamma_1 - K_g)d + K_d g^*, \quad (106b)$$

where

$$K_g = 2(2\alpha_P + \beta_P)\left[a^2\cos^2\phi + b^2\cos^2\left(\phi - \frac{2\pi}{3}\right) + c^2\cos^2\left(\phi + \frac{2\pi}{3}\right)\right] + 2\beta_P, \quad (107)$$

$$K_d = 2\beta_P\left[A^2\cos^2\phi + B^2\cos^2\left(\phi - \frac{2\pi}{3}\right) + C^2\cos^2\left(\phi + \frac{2\pi}{3}\right)\right]. \quad (108)$$

The stability conditions for AH patterns are

$$W > 0, \quad (109)$$

$$|2\alpha_P + \beta_P|^2 W^2 - 4|K_d|^2 > 0, \quad (110)$$

where

$$W \equiv 4[a^2\cos^2\phi + b^2\cos^2(\phi - 2\pi/3) + c^2\cos^2(\phi + 2\pi/3)] - 1.$$

Before performing the analysis of the conditions given by Eqs. (109) and (110), we recall that AR-A are unstable with respect to perturbations with $\phi \approx 0$, see Appendix B in Ref. [12]. (However, the growth rate for this mode is proportional to $L^2$ and consequently is rather small.) Therefore, AH close to ARs must be unstable as well.

Applying the triangle inequality, it is possible to show that the first condition is valid for any value of $\phi$ and any AH pattern. However, the minimal value of $W$ is equal to zero; it is approached for ARs, when one of the amplitudes vanishes.

Consider the second condition, given by Eq. (109). Because of the fact that $|\alpha_P| \gg |\beta_P|$ for sufficiently small values of the Lewis number, this inequality is met except for the situation where $W$ is small, that is, AH close to an unstable AR. Asynchronous hexagons close to AR-A are analyzed in Appendix D. It is shown that there exists a narrow interval of $\Phi - \Psi$ close to $\pi$, where AH are unstable. Another case when Eq. (110) may be violated is that of a small value of $|\chi|$. This case is considered in Appendix D as well.

### B. Instability on a superlattice

It is clear that perturbations with $\phi = \pi/2$ should be considered separately. Indeed, their interaction with the waves with wave vectors $\pm\mathbf{K}^{(1)}$ produces the "oblique" waves with wave vectors $k\,(\pm 1,\ 1)$ and the frequency $2\tilde{\Omega}$, which also meet the resonant conditions [Eqs. (24)] for $s_1 = s_2 = 1$, $s_3 = 0$. The oblique waves, in turn, interact with the same base waves, influencing the perturbation. Accounting for the emergence of

the oblique waves, we derive the following stability conditions for AH:

$$T_r > 0, \qquad (111)$$
$$|T| > 3|\beta_P|a^2,$$
$$T = (2\alpha_P + \beta_P)(2S_0 - 3a^2) + \frac{4\mu_1\mu_2 a^2}{\Gamma_2 - 2i\gamma_{0i}},$$
$$\mu_1 = \mu^{(1)} + \mu^{(2)}, \quad \mu_2 = 2\mu^{(1)} + 2\mu^{(2)}\left(1 + \frac{2}{P}\right), \qquad (112)$$
$$\mu^{(1)} = \frac{m_0^2\chi}{20L}\left(1 + \frac{i}{\Omega}\right),$$
$$\mu^{(2)} = \frac{m_0^2}{20}\left[1 + \chi + \frac{i}{\Omega}(\chi + L + \chi L)\right],$$

where $\Gamma_2 \equiv \gamma(\sqrt{2}k)$, $S_0 = a^2 + b^2 + c^2$. There are of course two similar conditions of stability when $a$ is replaced with $b$ or $c$. Due to the triangle inequality, we obtain $2b^2 + 2c^2 - a^2 \geqslant a^2$, that is, the first condition is weaker than the condition for supercritical bifurcation for alternating rolls on a square lattice, ARS {cf. Eq. (65) and Fig. 2 in Ref. [12]}. The second condition is satisfied everywhere except for a narrow interval of the Soret number $|\chi| = O(L^2)$, see Appendix D.

These results were confirmed by numerical solution of the amplitude equations. We solve the amplitude equations for the superlattice, representing $h$ as a superposition of 12 traveling waves with their wave numbers tilted at angles $n\pi/6$ ($n = 0, \ldots, 11$). Such a superlattice includes both square and hexagonal lattices and allows us to study the pattern selection. Our numerical computations show that the system approaches either square patterns (ARS) or AH. Thus, these numerical results confirm the stability of AH with respect to square patterns.

Summarizing this, a three-parameter family of AH is stable with the following three exceptions:

(i) AH close to ARs.

(ii) All solutions of the AH type are unstable for small values of the Soret number $|\chi| = O(L^2)$.

(iii) All AH patterns are unstable with respect to square patterns for Schmidt numbers of order one and $\chi \approx -1$, when subcritical bifurcation takes place for ARS.

Concluding this section, we emphasize that one of the patterns forming a heteroclinic cycle (AR) is unstable with respect to the external perturbations. However, for small $L$ the growth rate is rather small for AR and instability of AR does not necessarily break the heteroclinic connection. As mentioned in Appendix D, the growing perturbation mode can be adequately described in terms of modulation of AR. Analysis of the heteroclinic cycle in this case lies outside the scope of this paper.

## VIII. CONCLUSIONS AND DISCUSSION

We have studied oscillatory long-wave Marangoni convection in a layer of binary mixture in the presence of the Soret effect; in particular, pattern selection on a hexagonal lattice is carried out.

In addition to the degeneracy of the set of amplitude equations with cubic nonlinearity, revealed by Roberts *et al.* [7], we have found the novel degeneracy, which is inherent to a wide class of problems, where a long-wave oscillatory mode exists. Due to the degeneracy, an entire three-parameter family of solutions is stable in the framework of the cubic amplitude equations.

In order to select the stable patterns within this family of patterns, we proceed to the next order, accounting for the quintic nonlinearity. Analysis of the derived set of amplitude equations demonstrates that either wavy rolls 2 (WR2) is a sole stable pattern or there are no stable patterns and a heteroclinic cycle AR→WR2→TwR→AR emerges. The system rambles between these three oscillatory patterns (limit cycles) being alternately attracted to and then repelled from each of them. It is also worth noting that the details of the dynamics are governed by $\ln\delta$, where the supercriticality $\delta$ is treated as a formal small parameter.

We have constructed the global map for the trajectory close to this cycle and have found its stability. The interesting feature of the heteroclinic cycle is that the duration of each loop grows *linearly* with its occurrence, instead of a usual *exponential* growth. As a consequence, the minimal distance between each unstable limit cycle forming the heteroclinic cycle decreases *exponentially* rather than *superexponentially* with the number of the loop.

Stability analysis with respect to external perturbations, which do not belong to the hexagonal lattice, performed for these three limit cycles results in the following: symmetric patterns, TwR and WR2, are stable in a wide range of parameters, whereas AR are unstable. However, the corresponding growth rate is proportional to $L^2$, which is small for most of liquid binary mixtures; therefore heteroclinic cycles may be experimentally observable.

Note that we have carried out the stability analysis only with respect to the perturbations of a fixed wave number. More general analysis involving a possible modulation of the hexagonal patterns is also needed. This will yield the dependence of the Fourier amplitudes $A_j$, $B_j$, and $C_j$, which enters into Eq. (20) on the slowest coordinates $X_1 = \delta X$ and $Y_1 = \delta Y$. Our preliminary calculations show that in this case, a production of the "mean" (depending on $X_1$ and $Y_1$ only) parts of both the temperature and concentration perturbations is unimportant; the same is valid for the mean toroidal component of the flow. Therefore, in order to take the modulations into account, one only has to add advective $\pm\delta^{-1}V\partial_{X_1}A_{1,2}$ and diffusive $D\partial_{X_1}^2 A_{1,2}$, $-(iV/2k_c)\partial_{Y_1}^2 A_{1,2}$ terms to Eqs. (29), where real $V$ and complex $D$ can be readily extracted from the growth rate $\gamma(k)$. (Similar equations for $B_j$ and $C_j$ are obvious.) The presence of large advective terms inherent to the complex Ginzburg-Landau equations [4] drastically changes the situation in comparison to the case considered by Roberts *et al.* [7]. However, this study is beyond this paper.

## ACKNOWLEDGMENTS

This work is partially supported by the European Union via FP7 Marie Curie scheme Grant PITN-GA-2008-214919 (MULTIFLOW). A.O. was also partially supported by the Grant No. 2008038 from the Binational Science US–Israel

Foundation and by Fund for Promotion of Research at the Technion.

## APPENDIX A: LIMIT CYCLES IN THE FRAMEWORK OF EQS. (25)

For the sake of convenience we present 11 limit cycles found for the set of amplitude equations [Eqs. (25)] by Roberts *et al.* [7] as well as the limit cycle revealed by Swift [16]. Hereafter we adopt the classification of the patterns suggested by Clune and Knobloch [8] with the only exception for alternating rolls. Following these papers, we indicate only a representative for each group orbit; the remaining limit cycles forming the group orbit can be easily obtained by obvious transformations, such as interchanging subscripts 1 and 2 or/and cyclic permutation of $a$, $b$, and $c$.

All complex amplitudes are represented in the form given by Eq. (31), and the notation in terms of the phase differences $\Phi$, $\Psi$, $\Delta$, see Eqs. (32), is used. The values of the phase differences are indicated only when they are necessary, otherwise any value of the corresponding variable can be chosen.

The six among the limit cycles listed by Roberts *et al.* [7] belonging to the rhombic (rectangular) lattice are:

(i) Traveling rolls (TR):

$$a_1 \neq 0, \quad a_2 = b_j = c_j = 0;$$

(ii) standing rolls (SR):

$$a_1 = a_2 \neq 0, \quad b_j = c_j = 0;$$

(iii) traveling rectangles 1 (TRa1):

$$a_1 = b_1 \neq 0, \quad a_2 = b_2 = c_j = 0;$$

(iv) traveling rectangles 2 (TRa2):

$$a_1 = b_2 \neq 0, \quad a_2 = b_1 = c_j = 0;$$

(v) standing rectangles (SRa):

$$a_j = b_j \neq 0, \quad \Phi = 0, \quad c_j = 0;$$

(vi) alternating rolls (AR):

$$a_j = b_j \neq 0, \quad \Phi = \pi, \quad c_j = 0.$$

The last pattern coincides with wavy rolls 1 (WR1) in classification of Ref. [8]. This coincidence can be demonstrated by an appropriate shift of the origin. Indeed, it is obvious that the WR1 pattern with $A_1 = A_2 = B_1 = -B_2$ can be transformed into AR with $A_1 = A_2 = iB_1 = iB_2$ by $X \to X + \pi/k$.

Besides, an additional pattern revealed by Swift [16] also exists under certain conditions on a rhombic and, hence, on a hexagonal lattice:

(vii) Standing cross rolls (SCR):

$$A_1 = A_2 \neq 0, \quad B_1 = B_2 \neq 0, \quad a_1 \neq b_1, \quad c_j = 0.$$

(For SCR, $\Phi$ has a certain value which depends on $a_1 - b_1$.) However, this pattern is known to be unstable [6].

The remaining five (genuine hexagonal) patterns are:

(viii) Oscillating triangles (OT):

$$a_1 = b_1 = c_1 \neq 0, \quad a_2 = b_2 = c_2 = 0;$$

(ix) standing hexagons (StH):

$$a_j = b_j = c_j \neq 0, \quad \Phi = \Psi = 0, \quad \Delta = 0;$$

(x) standing regular triangles (SRT):

$$a_j = b_j = c_j \neq 0, \quad \Phi = \Psi = 0, \quad \Delta = \pi;$$

(xi) twisted rectangles (TwR):

$$a_j = b_j = c_j \neq 0, \quad \Phi = \Psi = 2\pi/3, \quad \Delta = 0;$$

(xiii) wavy rolls 2 (WR2):

$$a_j = b_j = c_j \neq 0, \quad \Phi = \Psi = 2\pi/3, \quad \Delta = \pi.$$

We do not present here the snapshots and the stability properties of these patterns, which can be found in Ref. [7] (see also a brief summary in Ref. [8]).

## APPENDIX B: GENERAL CASE OF AMPLITUDE EQUATION WITH THE CUBIC NONLINEARITY

Here we consider an arbitrary problem which allows *long-wave oscillatory* mode. The sole limitation is that a complex amplitude $h$ is determined up to an additive constant, that is, only $\nabla h$ influences the nonlinear dynamics. Recall that for the long-wave mode $|\nabla h| \ll |h|$.

Consider the coefficient which characterizes nonlinear interaction of three waves, $A_{\mathbf{k}_1}$, $A_{\mathbf{k}_2}$, and $A_{\mathbf{k}_3}$ producing the wave $A_{\mathbf{k}}$ of such kind that $s_1 = s_2 = -s_3 = 1$ in the resonant condition [Eqs. (24)]. (Later on we denote this type of interaction as $A_{\mathbf{k}_1} + A_{\mathbf{k}_2} - A_{\mathbf{k}_3} \to A_{\mathbf{k}}$.) The general form of a scalar coefficient for such an interaction is

$$K = \tilde{\alpha}_P(\mathbf{k}_1 \cdot \mathbf{k}_2)(\mathbf{k}_3 \cdot \mathbf{k}) + \tilde{\beta}_P(\mathbf{k}_1 \cdot \mathbf{k}_3)(\mathbf{k}_2 \cdot \mathbf{k}) + \tilde{\beta}_P(\mathbf{k}_2 \cdot \mathbf{k}_3)(\mathbf{k}_1 \cdot \mathbf{k}). \tag{B1}$$

Indeed, this form takes into account all scalar combinations of the wave vectors which have the minimal (fourth) order with respect to the wave numbers. The coefficients at the second and third terms are equal to each other in order to provide the invariance of $K$ with respect to the interchange of the subscripts $1 \leftrightarrow 2$.

Next, we restrict ourselves by the consideration of the problem with a certain nonzero critical wave number $k$. Therefore, near the stability threshold all the interacting waves have the wave vectors of equal length $k$. It is known from Ref. [10] that for the interaction of waves with equal wave numbers $k$, only two types of interactions satisfy the resonant conditions (24):

(i) $\mathbf{k}_3 = \mathbf{k}_1, \quad \mathbf{k}_2 = \mathbf{k}$;

(ii) $\mathbf{k}_2 = -\mathbf{k}_1, \quad \mathbf{k}_3 = -\mathbf{k}$.

In case (i) one obtains

$$K_1 k^{-4} = (\tilde{\alpha}_P + \tilde{\beta}_P)\cos^2\theta + \tilde{\beta}_P,$$

where $\theta$ is the angle between wave vectors $\mathbf{k}$ and $\mathbf{k}_1$. In particular, for $\theta = \pi$

$$2K_0 k^{-4} = \tilde{\alpha}_P + 2\tilde{\beta}_P.$$

(It is shown in Ref. [10] that the self-interaction coefficient $\theta = 0$ is a half of cross-interaction coefficient for $\theta = \pi$.)

For case (ii)

$$K_2 k^{-4} = \tilde{\alpha}_P + 2\tilde{\beta}_P \cos^2\theta.$$

Setting $\tilde{\alpha}_P k^4 = 2\alpha_P$ and $\tilde{\beta}_P k^4 = \beta_P$, one immediately arrives at Eq. (37) of Ref. [12], or at their corollary for $\theta = 2\pi/3$ [Eq. (26)]. Therefore, we obtain Eq. (26) based upon the general form of the coefficient Eq. (B1) and resonant conditions Eqs. (24).

## APPENDIX C: GENERAL EQUATIONS WITH CUBIC NONLINEARITY

Consider Eqs. (25) for arbitrary regimes by relaxing the conditions $a_1 = a_2$, $b_1 = b_2$, and $c_1 = c_2$. Using an exponential representation of the complex amplitude [Eq. (31)] and introducing new variables

$$P_a = a_1^2 + a_2^2, \quad P_b = b_1^2 + b_2^2, \quad P_c = c_1^2 + c_2^2, \tag{C1}$$

$$Q_a = a_1^2 - a_2^2, \quad Q_b = b_1^2 - b_2^2, \quad Q_c = c_1^2 - c_2^2, \tag{C2}$$

we obtain a set of equations

$$\partial_{\tau_1} P_a = 2\gamma_{1r} P_a - 2\alpha_{Pr} S P_a - \alpha_{Pr} Q_a^2 - 2\mathrm{Re}(K_2 \hat{\Sigma})\sqrt{P_a^2 - Q_a^2}, \tag{C3a}$$

$$\partial_{\tau_1} P_b = 2\gamma_{1r} P_b - 2\alpha_{Pr} S P_b - \alpha_{Pr} Q_b^2 - 2\mathrm{Re}(K_2 e^{i\Phi} \hat{\Sigma})\sqrt{P_b^2 - Q_b^2}, \tag{C3b}$$

$$\partial_{\tau_1} P_c = 2\gamma_{1r} P_c - 2\alpha_{Pr} S P_c - \alpha_{Pr} Q_c^2 - 2\mathrm{Re}(K_2 e^{i\Psi} \hat{\Sigma})\sqrt{P_c^2 - Q_c^2}, \tag{C3c}$$

$$\partial_{\tau_1} Q_a = (2\gamma_{1r} - \alpha_{Pr} P_a - 2\alpha_{Pr} S) Q_a, \tag{C3d}$$

$$\partial_{\tau_1} Q_b = (2\gamma_{1r} - \alpha_{Pr} P_b - 2\alpha_{Pr} S) Q_b, \tag{C3e}$$

$$\partial_{\tau_1} Q_c = (2\gamma_{1r} - \alpha_{Pr} P_c - 2\alpha_{Pr} S) Q_c, \tag{C3f}$$

$$\partial_{\tau_1} \Phi = 2\left[\frac{P_b \mathrm{Im}(K_2 \hat{\Sigma} e^{i\Phi})}{\sqrt{P_b^2 - Q_b^2}} - \frac{P_a \mathrm{Im}(K_2 \hat{\Sigma})}{\sqrt{P_a^2 - Q_a^2}}\right], \tag{C3g}$$

$$\partial_{\tau_1} \Psi = 2\left[\frac{P_c \mathrm{Im}(K_2 \hat{\Sigma} e^{i\Psi})}{\sqrt{P_c^2 - Q_c^2}} - \frac{P_a \mathrm{Im}(K_2 \hat{\Sigma})}{\sqrt{P_a^2 - Q_a^2}}\right], \tag{C3h}$$

$$\partial_{\tau_1} \Delta = -2(K_0 - K_1)_i (Q_a + Q_b + Q_c) + 2\mathrm{Im}\left[K_2 \hat{\Sigma}\left(\frac{Q_a}{\sqrt{P_a^2 - Q_a^2}} + \frac{Q_b e^{i\Phi}}{\sqrt{P_b^2 - Q_b^2}} + \frac{Q_c e^{i\Psi}}{\sqrt{P_c^2 - Q_c^2}}\right)\right]. \tag{C3i}$$

Here $2\hat{\Sigma} = \sqrt{P_a^2 - Q_a^2} + e^{-i\Phi}\sqrt{P_b^2 - Q_b^2} + e^{-i\Psi}\sqrt{P_c^2 - Q_c^2}$, $2S = P_a + P_b + P_c$. These variables coincide with those defined by Eqs. (30) and (38) for $Q_a = Q_b = Q_c = 0$. The phase differences $\Phi$, $\Psi$, and $\Delta$ are given by Eqs. (32).

It is readily seen that a limit cycle corresponding to AH with $P_a = 2a^2$, $P_b = 2b^2$, $P_c = 2c^2$, $Q_a = Q_b = Q_c = 0$ and with arbitrary values of $\Phi$, $\Psi$, satisfying conditions given by either Eqs. (43) or (44), is stable with respect to perturbations of $Q_a$, $Q_b$, $Q_c$ breaking the symmetry of standing waves. Note that other perturbations can be analyzed in the framework of the symmetrized set of Eqs. (37).

For example, the growth rate for a disturbance of $Q_a$ is determined by

$$\lambda = -2\alpha_{Pr} a^2 < 0. \tag{C4}$$

The same is valid for perturbations of $Q_b$ and $Q_c$.

## APPENDIX D: EXTERNAL PERTURBATIONS FOR AH

It was shown in Ref. [12] that AR-Rs with $\theta = \pi/3$, that is, ARs on the hexagonal lattice, are unstable with respect to external perturbations. Thus we first consider the condition given by Eq. (110) for small $L$ and for AH close to AR-A, $\Phi - \Psi \approx \pi$:

$$\Phi = \frac{\pi}{2} + \Delta_\Phi + \delta_\Phi, \tag{D1}$$

$$\Psi = -\frac{\pi}{2} + \Delta_\Phi - \delta_\Phi, \quad \delta_\Phi \ll 1, \tag{D2}$$

$$\phi = \pi n + \delta_\phi, \quad \delta_\phi \ll 1, \quad n = 0, 1, \tag{D3}$$

which provides small values for $W$.

The small parameter $\delta_\Phi$ characterizes the distinction between the AH pattern under consideration and AR. Note that due to Eqs. (43) and (44), $\delta_\Phi \geqslant 0$ and $|\Delta_\Phi| \leqslant \pi/2$. It should be also emphasized that $\phi$ is close to either zero or $\pi$, that is, the perturbation represents a transverse modulation of the smallest standing wave. In fact, analysis of a longitudinal modulation, slightly violating the condition $k = k_c$, is also pertinent.

Substituting these expressions into Eq. (110) and keeping only leading terms, we obtain

$$m_0(m_0 - 1)\left(3\delta_\Phi + 2\cos\Delta_\Phi \delta_\phi^2\right)^2 - 12\cos^2\Delta_\Phi \delta_\phi^2 L^2 > 0. \tag{D4}$$

This inequality is satisfied for any $\delta_\phi$ at

$$\delta_\Phi > \frac{L^2}{2m_0(m_0 - 1)} \geqslant \frac{L^2 \cos\Delta_\Phi}{2m_0(m_0 - 1)}. \tag{D5}$$

Clearly, a similar instability takes place for $\Phi \to \pi$ with $c \ll 1$ or for $\Psi \to -\pi$ with small $b$. Thus, for sufficiently small values of the Lewis number only AH close to ARs with $\theta = \pi/3$ are unstable.

The second possibility to violate Eq. (110) is the above-mentioned case of small $|\chi|$. Introducing $\chi_L \equiv -\chi L^{-2} - 1$, $\chi_L > -(L + L^2)/(1 + L + L^2)$, we obtain the following condition of stability for AH:

$$\chi_L > \frac{3|\sqrt{3}a^2\cos 2\phi - (b^2 e^{-i\Phi} - c^2 e^{-i\Psi})\sin 2\phi|^2}{[S_0 + (3a^2 - S_0)\cos 2\phi + \sqrt{3}(b^2 - c^2)\sin 2\phi]^2} - 4. \tag{D6}$$

Here, again, $S_0 = a^2 + b^2 + c^2$.

Analysis of this condition shows that for any values of $\Phi$, $\Psi$, there exists a value of $\phi$, so that the right-hand side of Eq. (D6) is positive, that is, each AH from a three-parameter family is unstable for extremely small $|\chi|$, $|\chi| = O(L^2)$. Of course the right-hand side of Eq. (D6) diverges for either $\Psi = -\pi$ or $\Phi = \pi$ or $\Phi - \Psi = \pi$, that is, when AH degenerates to the unstable ARs.

Analysis of condition (112) in the same limiting case for finite values of the Prandtl number results in the following inequality:

$$\chi_L > \frac{(9a^2 - 4S_0)(4S_0 - 3a^2)}{(2S_0 - 3a^2)^2}, \tag{D7}$$

that is, AH with $5a^2 > 4(b^2 + c^2)$ are unstable with respect to squares for small $|\chi|$. However, the latter condition is embedded in Eq. (D6).


[1] R. B. Hoyle, *Pattern Formation: An Introduction to Methods* (Cambridge University Press, Cambridge, 2006).
[2] L. M. Pismen, *Patterns and Interfaces in Dissipative Dynamics* (Springer, Berlin, 2006).
[3] A. A. Nepomnyashchy, M. G. Velarde, and P. Colinet, *Interfacial Phenomena and Convection* (Chapman and Hall/CRC, London, 2001).
[4] I. S. Aranson and L. Kramer, Rev. Mod. Phys. **74**, 99 (2002).
[5] Y. Pomeau, Physica D **23**, 3 (1986).
[6] M. Silber and E. Knobloch, Nonlinearity **4**, 1063 (1991).
[7] M. Roberts, J. W. Swift, and D. H. Wagner, Contemp. Math. **56**, 283 (1986).
[8] T. Clune and E. Knobloch, Physica D **74**, 151 (1994).
[9] A. Oron and A. A. Nepomnyashchy, Phys. Rev. E **69**, 016313 (2004).
[10] L. M. Pismen, Phys. Rev. A **38**, 2564 (1988).
[11] T. Clune, M. C. Depassier, and E. Knobloch, in *Instabilities and Nonequilibrium Structures*, edited by E. Tirapegui and W. Zeller (Kluwer Acdemic, Netherlands, 1996), p. 75.
[12] S. Shklyaev, A. A. Nepomnyashchy, and A. Oron, Phys. Fluids **19**, 072105 (2007).
[13] S. Shklyaev, A. A. Nepomnyashchy, and A. Oron, Europhys. Lett. **86**, 14005 (2009).
[14] A. Podolny, A. A. Nepomnyashchy, and A. Oron, Phys. Rev. E **76**, 026309 (2007).
[15] S. Shklyaev, A. A. Nepomnyashchy, and A. Oron, Phys. Fluids **21**, 054101 (2009).
[16] J. W. Swift, Nonlinearity **1**, 333 (1988).
[17] T. P. Lyubimova and Y. N. Parshakova, Fluid Dyn. **42**, 695 (2007).
[18] M. Krupa and I. Melbourne, Ergod. Theor. Dyn. Syst. **15**, 121 (1995).
[19] V. Kirk and M. Silber, Nonlinearity **7**, 1605 (1994).
[20] I. Melbourne, P. Chossat, and M. Golubitsky, Proceedings of the Royal Society of Edinburgh Section A-Mathematics **113**, 315 (1989).
[21] E. Stone and P. Holmes, SIAM J. Appl. Math. **50**, 726 (1990).
[22] F. M. Busse and K. E. Heikes, Science **208**, 173 (1980).